



Enhanced Removal of Salbutamol in Water Solution Using Cu-Based Magnetic Designed Metal–Organic Frameworks: Kinetics and Isothermal Models and Statistical Analysis

Usman Armaya^{1,2} · Marinah Mohd Ariffin¹ · Saw Hong Loh¹ · Wan Mohd Afiq Wan Mohd Khalik¹ · Nurhanna Badar^{1,3} · Kelimah Elong⁴ · Hanis Mohd Yusoff^{1,3}

Received: 6 February 2023 / Accepted: 24 July 2023 / Published online: 21 August 2023
© King Fahd University of Petroleum & Minerals 2023

Abstract

Clean water quality is dependent on the absence or complete removal of polar ionic micropollutant molecules and their associated products from the water. Utilizing copper Isonicotinate metal–organic frameworks ([Cu (INA)-MOF) a modified copper-based magnetic composite metal–organic framework ([Cu (INA)₂]-MOF@Fe₃O₄) is mechanically synthesized under environmentally friendly conditions, and an adsorptive removal of salbutamol in water was successfully achieved in both synthesized materials. Characterization toward the materials has been carried out using X-ray diffraction, Brunauer–Emmett–Teller, field emission scanning microscopy, scanning electron microscopy, thermogravimetric analysis, and Fourier transform infrared spectroscopy. Our synthesized ([Cu (INA)₂]-MOF@Fe₃O₄) used as an adsorbent in water showed enhanced performance in the removal of the model salbutamol within a shorter contact time (40 min) with the pseudo-second-order and Langmuir models providing the most accurate statistical descriptions of the process's kinetics and isotherms, respectively, while thermodynamic studies indicated that the process was endothermic, spontaneous, and the material demonstrated very good reusability and regeneration with a very good percentage recovery even after the fifth cycle.

Keywords Salbutamol · β -agonists · Magnetic composite · Metal–organic frameworks · Adsorption · Kinetic and isothermal models

1 Introduction

A review of the occurrences of β -agonists compounds in surface water, groundwater, and drinking water indicated a sharp increase in their concentrations over the days, thereby developing into a severe problem during the last two decades and has recently been presented by our research group [1].

The accumulation of β -agonists concentration in our drinking water is scientifically proven to trigger variety of health problems to humanity causing symptoms such as tachycardia, nervousness, muscle tremors, fatigue, confusion, headache, dizziness, chest distress, heart palpitations, anxiety, insomnia, itching, and limb numbness [2, 3], as well as other abnormal conditions such as fibrillation, which is particularly prevalent in hypertense [4]. An additional clinical symptoms and signs can include chain pains and severe pain at the injection sites [5].

β -Adrenergic agonists are adrenergic receptors that were first utilized in human treatment in the 1970s and are now routinely used for bronchodilation and other purposes mostly found in the heart, lungs, and blood vessels [6]. Given its ability to provide repartitioning effects and improve glucose homeostasis in humans with insulin resistance and diabetes, it has been proposed as a potential therapy to treat muscle deterioration and a potential anti-diabetic agent in humans. β -agonists as a drug are allowed for use in individuals with asthma in Europe at a dosage of 20–40 mg orally, twice a day,

✉ Hanis Mohd Yusoff
hanismy@umt.edu.my

¹ Faculty of Science and Marine Environment, Universiti Malaysia Terengganu, 21030 Kuala Nerus, Terengganu, Malaysia

² Faculty of Applied Sciences, Al-Qalam University Katsina, Katsina, Nigeria

³ Advanced Nano Materials (ANoMa) Research Group, Faculty of Science and Marine Environment, Universiti Malaysia Terengganu, 21030 Kuala Nerus, Terengganu, Malaysia

⁴ Centre for Functional Materials and Nanotechnology, Institute of Science, Universiti Teknologi MARA, 40450 Shah Alam, Selangor, Malaysia



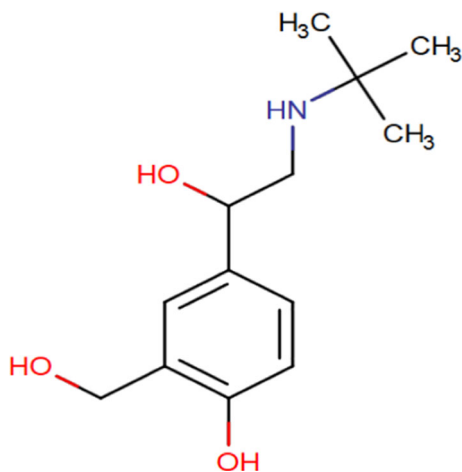


Fig. 1 Salbutamol

according to the European Medicines Agency [5]. They are partly metabolized in the body and eliminated in the urine either as the original drug or as metabolites of the original substance, as reports indicated their 60–70% excretion into the environment in their unmetabolized form [7–9]. Consequently, they are released into the environment through urban wastewater. Due to their hydrophilic nature and limited separation at wastewater treatment plants (WWTPs) and drinking water treatment plants, many of these contaminants can spread further through the water cycle, eventually reaching groundwater and into our drinking water.

β -agonists, as polar, ionizable, and nonvolatile compounds, happened to be among the most difficult micro-contaminants to remove from the environment, especially given their constant daily introduction into the environment, as their polarity facilitates their spread in water [10].

Salbutamol (Fig. 1), is one of the major β -agonists drugs with the chemical name; 2-(ter-butylamino)-1-(4-hydroxymethylphenyl) ethanol, with molecular formula represented as $C_{13}H_{21}NO_3$, water solubility as low as 2.15 mg/mL, a pK_a of 9.83 ± 0.47 [10, 11] and structural representation in Fig. 1. Detection of a free salbutamol concentration in urine exceeding 1 g/mL, is considered a doping violation for its ergogenic aids ability [1].

Chemical and biological methods, such as oxidation [12, 13], photodegradation [9, 14], and adsorption [15], have all been used to accomplish the removal of β -agonists in our environmental waters. But for the reason that such techniques as oxidation and photocatalytic degradation frequently produce intermediates with toxicity greater than that of the pollutants, adsorption is considered to be the most favorable as its simple, promising, inexpensive, and environmentally friendly method of eliminating pollutants during wastewater recovery [16]. Adsorption, on the other hand, is dependent on the adsorbent, i.e., its adsorption capability, contact

time, adsorbent dose, and pH variations [17], so the principal downsides of several adsorption techniques are the opposite of the aforementioned qualities as poor adsorption capacities, extended contact times, high dose, and pH values that are either very low or excessively high. So far only few documented studies on adsorbents used for the removal of salbutamol in our environmental water were available, viz., granular activated carbon (GAC) [15], micro-grain activated carbon (μ -GAC) [18], and anionic cellulose nanofibrils (CNFs) [19]. Most of these studies, on the other hand, had poor adsorption efficiency, a prolonged equilibrium time up to around some weeks to attain, and were difficult to regenerate or some studies did not have any record of regenerations.

Metal–organic frameworks (MOFs) have made tremendous development in recent years owing to their diverse structure and a large variety of application possibilities [20]. MOFs are a type of nanoporous materials with metal-based building units that are coordinated with organic bridging ligands to form an interconnected 3-D network with a uniform pore system that includes channels and enclosures with openings that typically range from 3 to 90 microns in size through which you can construct MOF structures that have the desired structural characteristics [21]. Through the use of these specific three-dimensional connectivity between inorganic and organic units, it is possible to create MOF architectures with low framework densities (from 0.2 g/cm^3), high void volumes (up to 90%), and as a result of the very porous structure formed by the crystalline ordering of the components, the interior specific surface areas reach over thousands of m^2/g , which is extremely large, these are all among the MOFs' most attractive features [17, 22, 23]. Hariz [24] also discovered that the stability of MOFs was determined by the existence of hydrophobic functional groups, a high number of positive charges per atom, and the capacity to resist coordination with water molecules.

Their interest in both scientific and technological fields is as a result of their versatility in a variety of fields such as liquid adsorption [25], catalysis [23, 26] and sensing [27], electrochemistry and conversions [28] as well as in biomedical applications as contrasting agents and drug delivery [29]. The capacity to create tunable cavities with tailorable chemistry opens the door to a plethora of new possibilities for the development of materials with specific features such as the composite-MOF. When a composite is formed, it is a multi-component material that contains many phases and at least one continuous phase.

The synthesis, kinetics, morphology, physicochemical characteristics, stability, and possible applications of MOFs may all be significantly enhanced by functionalizing appropriate components into their composition [30]. By attaching active groups or impregnating appropriate active materials and altering the organic as well as fabricating composites

with suitable material, we can improve the physicochemistry of the materials. This development was extended by incorporation of magnetic nanomaterials into the MOFs' framework possible to create MOFs with magnetic properties as the one recently explored by Bellusci [22] in 2018. These MFCs exhibit vacant sites suitable for selective separation of the targeted compounds and also offer a magnetic separation ability. With much greater surface area than traditional materials, nano-magnetic structured adsorbents demonstrate significantly better efficiencies and quicker adsorption rates in water treatment as compared to conventional materials.

Further studies have shown that the incorporation of the second type of metal ion into the crystal lattice of a MOF containing a single type of metal ion is theoretically and practically feasible [31], resulting in a solid product that could be used to adjust the number or uniformity of SBU linkages between metal centers, resulting in a greater and controlled ordering of the mixed-metal ions into a crystalline MOF material that should display rich chemistry.

The adsorption of β -agonists from contaminated water can be accomplished using the physicochemical qualities of magnetic nanoparticles (i.e., particle sizes, surface area, surface charge, accumulation/aggregation, morphology, and surface coating) as well as chemisorption and/or physisorption features of MNPs.

A Cu-based magnetic composite metal–organic frameworks (MCMF) is mechano-synthesized using mortar, and pestle consisting of iron oxide nanoparticles (Fe_3O_4 -MNPs) is reported in this paper. Various characterization techniques such as Fourier transform infrared spectroscopy (FTIR), Brunauer–Emmett–Teller (BET), thermogravimetric analysis (TGA), X-ray diffraction (XRD), high-resolution transmission electron microscope (HR-TEM), and field emission scanning electron microscopy (FESEM) were all carried out on the synthesized materials. The specialized chemical functionalities of the magnetic composite-MOFs help in selectively adsorbing the salbutamol species which has special functional features that help in selective adsorption.

The studies of MCMF are very recent and its applications in water remediations, in general, are very few and no MCMF studies on β -agonists is so far reported. To the best of the author's knowledge, this is the first study based on MOFs and the MCMF on salbutamol adsorption from water. The green chemistry approach's synthesis is used here to develop functionalized materials through a process that eliminates or at least reduces hazardous waste generation that is harmful to human health and the environment, while also removing environmental pollutants (β -agonists) that are micro and non-volatile found in our environmental waters. The choice of making as well as using the copper-based MOF is because of the reported non-toxic effect of copper and the biocompatibility of the composite components, as well as their features

that were efficient for the ultimate application were taken consideration while selecting them.

2 Methodology

2.1 Chemicals and Materials

All chemicals used in this project were analytically assessed and utilized exactly as supplied. Sigma-Aldrich supplied the copper acetate monohydrate (98.5%), isonicotinic acid (98.5%), and salbutamol (St. Louis, MO, USA). Methanol (99.5%), sodium hydroxide, hydrochloric acid, iron(III) chloride hexahydrate (ferric chloride), and iron(II) chloride tetrahydrate (ferrous chloride) were all purchased from Sigma-Aldrich (St. Louis, MO, USA) and were supplied by IT Tech Research in Selangor, Malaysia.

2.2 Mechano-Synthesis of $[\text{Cu}(\text{INA})_2]$ -MOF

$[\text{Cu}(\text{INA})_2]$ -MOF was synthesized using a solvent-free approach similar to that described by Tella [32] with little modification. To summarize, 0.25 g (1 mmol) copper acetate monohydrate ($\text{Cu}(\text{CH}_3\text{COO})_2\text{H}_2\text{O}$) and 0.246 g (2 mmol) isonicotinic acid ($\text{C}_5\text{H}_4\text{N}(\text{CO}_2\text{H})$) were crushed together for 3 min using a mortar and pestle. The product's fabrication was followed by a familiar acetate characteristic odor and indications of a color change from green to blue. The resulting product was then heated for 12 h at 150 °C to eliminate the glacial acetic acid trapped in the pores of the copper isonicotinate MOF. The material (product) was placed in a desiccator to cool before being stored in a sample vial and afterward utilized without further treatment throughout the experimental procedure.

2.3 Mechano-Synthesis of the Fe_3O_4 -MNPs

Fe_3O_4 -MNPs were manufactured using an unusual mechanochemical approach, which was comparable to the one previously described by Bellusci [22, 33] with only minor modifications to the procedure. In a typical process, about 5 g of a molar ratio combination of reactants ($\text{FeCl}_3\cdot 6\text{H}_2\text{O}$, $\text{FeCl}_2\cdot 4\text{H}_2\text{O}$, and NaOH, all provided by Sigma-Aldrich) was mixed in a mortar and pestle until well combined. Sodium chloride was added in excess (to the tune of 100 wt%) to the stoichiometric mixture as a phase control agent to minimize the formation of crystalline development phenomena. The synthesis was completed by continually grinding the ingredients in a mortar and pestle. After 10 min of grinding, the materials combination was collected, and the powder was washed with water before being dried at 70 °C under vacuum and stored till further needed.



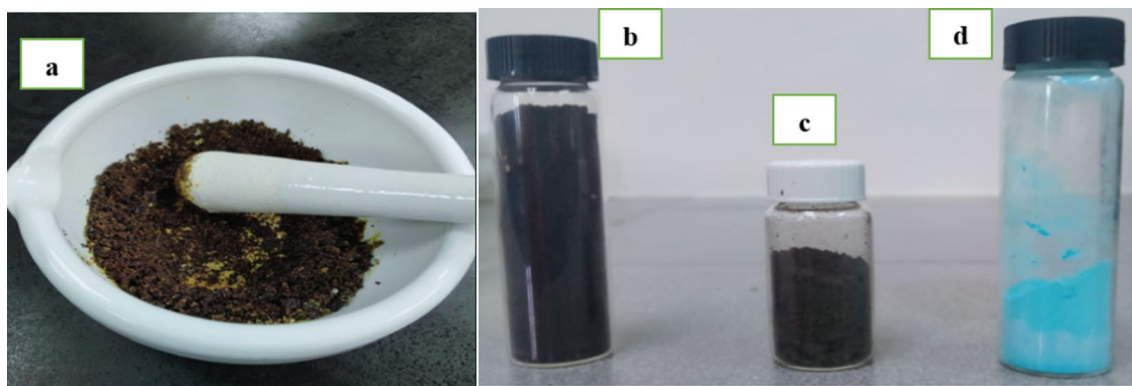
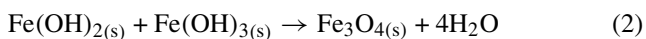
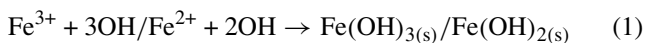


Fig. 2 a Mortar and pestle synthesis process of Fe_3O_4 -MNPs, b synthesized Fe_3O_4 -MNPs, and c synthesized $([\text{Cu}(\text{INA})_2]\text{-MOF})@\text{Fe}_3\text{O}_4$, and d synthesized $([\text{Cu}(\text{INA})_2]\text{-MOF})$

2.4 Mechano-Synthesis of the $([\text{Cu}(\text{INA})_2]\text{-MOF})@\text{Fe}_3\text{O}_4$ Using Mortar and Pestle

The Bellusci [22] procedure was followed with minor changes for the magnetic composite synthesis; in summary, Fe_3O_4 -MNPs was first decorated with $([\text{Cu}(\text{INA})_2]\text{-MOF})$ by neat grinding in a mortar using a pestle. Some 0.5 g of MNPs and 0.43 g of $([\text{Cu}(\text{INA})_2]\text{-MOF})$ were properly weighed into the mortar at the start. The combination was ground together for 10 min. The $\text{FeCl}_3 \cdot 6\text{H}_2\text{O}$ was then added, along with 2 mL of a water/ethanol combination (1:1 volume ratio), and the grinding was continued for another 10 min. Ethanol and water were used to purify the samples. Summarily, the magnetic composite was successfully functionalized with the Cu-MOF by neat grinding (Figs. 2, 9).

The complete equation for the reaction of the magnetic iron nanoparticles synthesis using the mechano-synthesis method is given below from Jannah [34].



2.5 Characterization of the Materials

Perkin–Elmer FTIR spectrometer was used for possible Fourier transformed infrared spectroscopy; the $([\text{Cu}(\text{INA})_2]\text{-MOF})$ and the $([\text{Cu}(\text{INA})_2]\text{-MOF})@\text{Fe}_3\text{O}_4$ were both characterized for its functional group identifications. The spectra of samples distributed in KBr pellets were evaluated in the $400\text{--}200\text{ cm}^{-1}$ range. A Shimadzu TGA-50 thermogravimetric analyzer was used to determine the thermal stability of the material, heating the material at $10\text{ }^\circ\text{C}/\text{min}$ in an inert atmosphere (Ar) or in air. The topography, microstructure, and elemental evidence were all determined using field emission scanning electron microscopy (FESEM) (Zeiss Supra

55 VP instrument). For high-resolution observation of the crystalline size and shape of the synthesized materials at nanoscale analysis, the high-resolution transmission electron microscope (HR-TEM) JEM-2100F multifunctional, 200 kV FE was used, and the determination of crystallinity was carried out using Bruker D8 Advance X-ray diffractometer to collect the X-ray diffraction patterns, with a 0.02° step width, data information was collected in the $4\text{--}50^\circ$ 2 range.

2.6 Removal Experimental Studies

2.6.1 Preparation of Salbutamol Solutions

Two milligram of salbutamol (100 mg/L) was dissolved in one 100 mL of methanol to yield a stock solution of salbutamol, after which the solution was kept refrigerated at $4\text{ }^\circ\text{C}$. Using milli-Q water, the working solutions were prepared daily right before the adsorption experiments and were obtained by dilution of the required stock solution to obtain the required amount. One of the advantages of using a mixture of methanol and water is that the surface tension and polarity of the water will both be reduced.

2.6.2 Batch Adsorption Study

The batch adsorption under one parameter at a time (OPAT) is the project's design of the experiment (DOE). Batch procedures are widely used because they are affordable and straightforward, making them appropriate for small and medium-sized process applications requiring simple and quickly accessible mixing container equipment. A series of adsorption experiments were carried out with both the two adsorbents at various concentrations following dilution of the stock solution with milli-Q water to make up the working solution. Each adsorbent $([\text{Cu}(\text{INA})_2]\text{-MOF})$ and the $([\text{Cu}(\text{INA})_2]\text{-MOF})@\text{Fe}_3\text{O}_4$ were individually suspended in a conical flask (150 mL) containing salbutamol solutions at



various starting concentrations ranging from 10, 20, 30, 40, 50 to 60 mg/L at the adsorbents' dose between 1, 2, 3, 4, 5 and 6 mg. It was then placed into a temperature regulated incubator shaker (stacked shaker SKE 8000) and agitated at a rate of 150 rpm for about 10–120 min. Approximately 2 mL of the sample solution was collected at 10-min intervals and filtered through a nylon syringe membrane (0.45 μm). The absorbance of analyte in the filtrate solution was determined using a UV–Visible spectrophotometer (Shimadzu UV-1800) at λ_{max} 283 nm using a quartz cuvette. The effect of pH was initially studied by adjusting the solution pH from pH 3, 5, 7, 9, 11 to pH 13 before reaching the final solution volume of 40 mL, the pH of the solution was controlled by adjusting to the appropriate value by adding a few drops of weak HCl or NaOH and the temperature influence was studied from 25, 30, 35, 40, 45 to 50 °C.

The percentage removal (% R), quantity adsorbed at a time (q_t), and quantity adsorbed at equilibrium (q_e) were calculated using Eqs. 3, 4, and 5 as described by [35] [36] as follows;

$$\%R = \frac{(C_0 - C_t)}{C_0} \times 100 \tag{3}$$

$$q_t = \frac{C_0 - C_t}{W} V \tag{4}$$

$$q_e = \frac{C_0 - C_e}{W} V \tag{5}$$

where C₀, C_t, and C_e are the initial concentration, concentration at a time (minute), and equilibrium concentration of salbutamol in mg/L, respectively, while W and V are the dry weight of the adsorbent and the volume of the solution (L), respectively.

The adsorption data in both the two adsorbents were obtained in triplicate, and the average results were calculated. The batch experiment's optimal parameters were determined to be pH 11, salbutamol concentration 40 mg L, adsorbent dosage 0.001 g L, temperature 25 °C, and contact time 40 min in a solution volume of 40 mL.

2.6.3 Regeneration and Reusability Study

The regeneration and reuse properties of the adsorbent were evaluated. After the adsorption research, the supernatant was decanted, and both the two adsorbents' residues were washed with 100% methanol (50 mL) and with distilled water before vacuum drying for 3 h at 100 °C and kept in the desiccator. The regenerated adsorbents were recycled for salbutamol adsorption at the optimal conditions developed in batch adsorption studies for five consecutive cycles.

2.7 Adsorption Isotherms

In this study, we used isotherm modeling to describe the equilibrium relationship between the adsorbate and the adsorbent that reflects the relative affinity of the two adsorbents to the salbutamol. We used the three most prominent isotherm models, which are described by the linear Eqs. (6), (7), and (8), to describe the equilibrium relationship between the two adsorbents and the salbutamol [35]

$$\frac{C_e}{q_e} = \frac{1}{K_L q_m} + \frac{1}{q_m} C_e \tag{6}$$

$$\log q_e = \log K_F + \frac{1}{n} \log C_e \tag{7}$$

$$q_e = \frac{RT}{b_T} \ln A_T + \left(\frac{RT}{b_T} \right) \ln C_e \tag{8}$$

where q_m is the adsorption capacity, K_L is the Langmuir constant, K_F is the Freundlich constant, and 1/n signifies the adsorption intensity, while b_T (kJ/mol) is the Temkin constant denoting the heat of adsorption, and A_T is the equilibrium binding constant denoting the maximum binding energy. The absolute temperature and the universal gas constant are denoted by T and R, respectively.

The above models were also fitted with statistical regression analysis to determine the coefficient of determination (R²), adjusted coefficient of determination (R² adj.), root mean square error (RMSE), and Akaike information criterion (AIC) as criteria to assess the model performance on the adsorption process, using Eqs. (9), (10), and (11) as the dataset [37].

$$R^2 = 1 - \frac{\sum (q_{eexp} - q_{ecal})^2}{\sum (q_{eexp})^2} \tag{9}$$

$$RMSE = \sqrt{\sum_{n=1}^i (q_{eexp} - q_{emodel})^2} \tag{10}$$

$$AIC = n \ln \left(\frac{SSE}{n} \right) + 2n_p + \frac{2n_p(n_p + 1)}{n(n_p + 1)} \tag{11}$$

where q_{e exp} and q_{e model} signify the adsorption capacities measured experimentally and numerically, respectively, n is the number of observations, and p signifies the number of parameters. The sum of square errors obtained is denoted by SSE. Generally, a piece of brief information summarized by these models conveys that the greater linearity of the models is shown by a higher R² value, but smaller RMSE and AIC values suggest better fitting of the models.

2.8 Kinetic Study

The kinetics research gives a thorough mechanism for the adsorption process as well as the rate-controlling stage in the process. So the information for salbutamol adsorption onto both the [Cu (INA)₂]-MOF and the [Cu (INA)₂]-MOF@Fe₃O₄ in this study was exposed to three of the most relevant models, namely pseudo-first-order, pseudo-second-order, and intraparticle diffusion represented by Eqs. (12), (13), and (14), respectively [35, 37].

$$\ln(q_e - q_t) = \ln q_e - k_1 t \quad (12)$$

$$\frac{t}{q_t} = \frac{1}{k_2 q_e^2} + \frac{t}{q_e} \quad (13)$$

$$q_t = K_P t^{1/2} + C \quad (14)$$

The amounts of salbutamol adsorbed at equilibrium and at a certain time are represented by the numbers q_e and q_t , respectively, while the pseudo-first-order and pseudo-second-order rate constants are represented by k_1 and k_2 , respectively. K_P is the intraparticle diffusion rate constant, while C denotes the constant of the system.

2.9 Thermodynamic Study

The thermodynamics analysis (of both the adsorbents) which is based on temperature differences, provides insight into the nature of the adsorption process and its parameters are conducted. According to Van't Hoff [38], the thermodynamic properties of the process, such as Gibbs free energy change (ΔG°), standard enthalpy change (ΔH°), and entropy change (ΔS°), were calculated using Eqs. (15), (16) and (17) according to Van't Hoff based on the temperature dependence of the adsorption process.

$$\Delta G^\circ = RT \ln K_d \quad (15)$$

$$K_d = \frac{q_e}{C_e} \quad (16)$$

$$\Delta G^\circ = \Delta H^\circ - T \Delta S^\circ \quad (17)$$

3 Result and Discussion

3.1 Characterizations

Thermograms of ([Cu (INA)₂]-MOF, Fe₃O₄-MNPs, and ([Cu (INA)₂]-MOF@Fe₃O₄) are presented in Fig. 3a, b, and c. The TG curves are shown as a function of % mass loss

over temperature. With an initial mass of 4.642 mg, the crystal MOF was exposed to TGA. The entire TG analysis was performed at a heating rate of 10.00 °C/min from 100.00 to 1000.00 °C. The [Cu (INA)-MOF complex was thermostable up to 250 °C, with an 82% weight loss at 246.38 °C and 322.66 °C [39], affirming the absence of a solvent molecule within the framework. The thermograms demonstrated that the [Cu (INA)₂]-MOF material has a good thermal resistance (Fig. 3a). Besides that, the Fe₃O₄-MNPs also showed two main losses of 5.8 (wt%) when heated to 245 °C, which can be related to the removal of water that was adsorbed on the particles' surface, and a further 2.25 mg was lost corresponding to weight loss of 12.76 (wt%) between 250 and thermally stable up to 950 °C, which can be attributed to the formation of hydroxyl groups [22], which resulted in the same major weight changes being recorded from both. While the thermogram of the Cu (INA)₂-MOFs@Fe₃O₄ (Fig. 3c) sample is very similar to that of the [Cu (INA)₂]-MOF, the only difference is the presence of the Fe₃O₄. The fact that the weight loss of [Cu (INA)₂]-MOFs@Fe₃O₄ is more efficient than that of [Cu (INA)₂]-MOF at temperatures ranging from 245 to 435 °C shows that the MOF accelerates the degradation of the iron oxide nanoparticles, which affects the thermal stability of the materials. However, the material we synthesized will be used at lower temperatures.

SEM images of the mechanically generated ([Cu (INA)-MOF crystalline phase with well-defined edges are shown (Fig. 4a). MOFs' porous nature is aided by their morphology, which consists of rectangular-square bars with a rough surface. The EDX of the [Cu (INA)₂]-MOF has revealed the surface elemental analysis of the material in Fig. 5e, which consists of Cu (13.93), C (48.41), N (13.05), and O (24.61); the obtained images match the composition of the previously published [Cu (INA)₂]-MOF [40, 41]. Furthermore, the ([Cu (INA)₂]-MOF@Fe₃O₄) images demonstrated extremely distinct morphological and topological features, as shown in Fig. 5b, c, while Fig. 5d presents an in-depth surface morphology of the Fe₃O₄ MNPs with pore openings at the outer surface and the elemental representations of the predicted elements in the material as revealed by EDX analysis, as shown in Fig. 5f.

TEM images of the [Cu (INA)₂]-MOF shown in Fig. 5 revealed that the samples were nanomaterials composed of irregular columnar, spherical, and cubic-structure nanoparticles that attach to and cluster together. The particle size of the samples was found to be between 5 and 20 nm.

Figure 6a, b, c, and d shows TEM images of Fe₃O₄-MNPs at different magnifications. The images revealed that the samples were nanomaterials made up of irregular columnar, spherical, and cubic-structure particles that adhered to each other and agglomerated. The particle size of the samples Fe₃O₄-MNPs have determined between 5 and 20 nm.

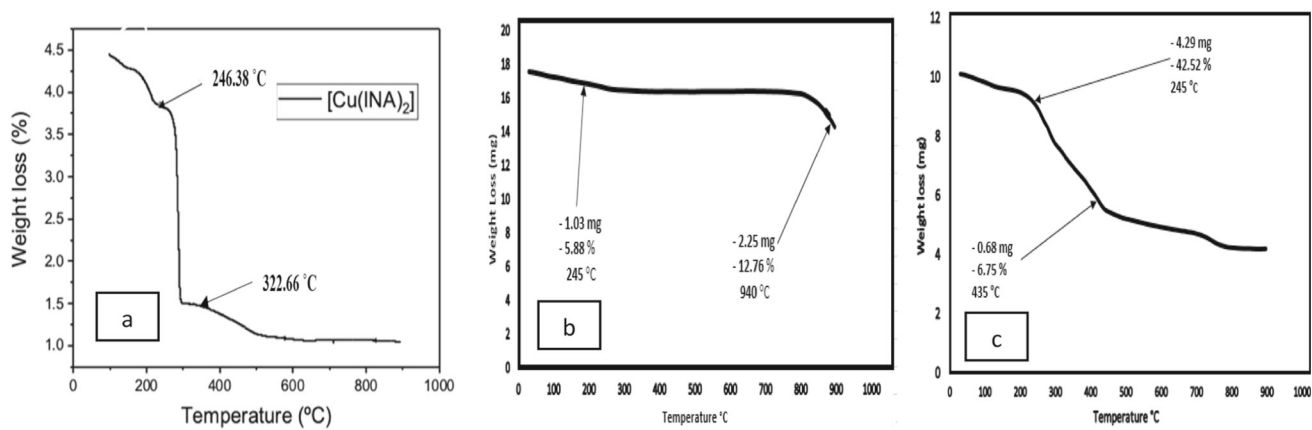


Fig. 3 Thermograms of **a** $[Cu(INA)_2]$ -MOF, **b** Fe_3O_4 -MNPs, and **c** MOFs ($Cu(INA)_2MOF@Fe_3O_4$)

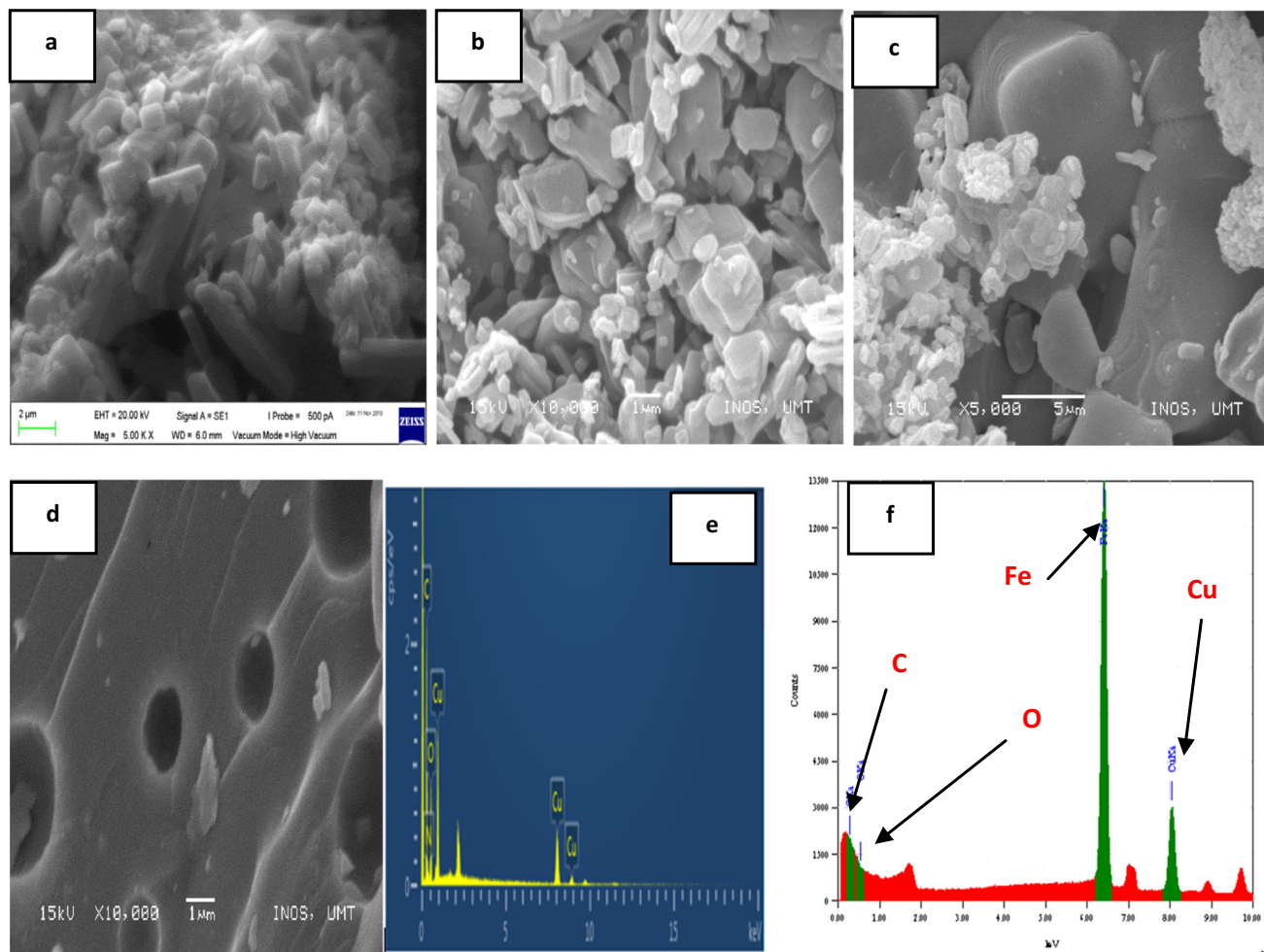


Fig. 4 SEM images of **a** $[Cu(INA)_2]$ -MOF, **b** $[Cu(INA)_2]$ -MOF@ Fe_3O_4 at 10 kV magnification, **c** $[Cu(INA)_2]$ -MOF@ Fe_3O_4 at 5 kV magnification, **d** Fe_3O_4 -MNPs at 10.00 kV magnification, **e** EDX spectra of the $[Cu(INA)_2]$ -MOF, and **f** EDX spectra of the $[Cu(INA)_2]$ -MOF@ Fe_3O_4

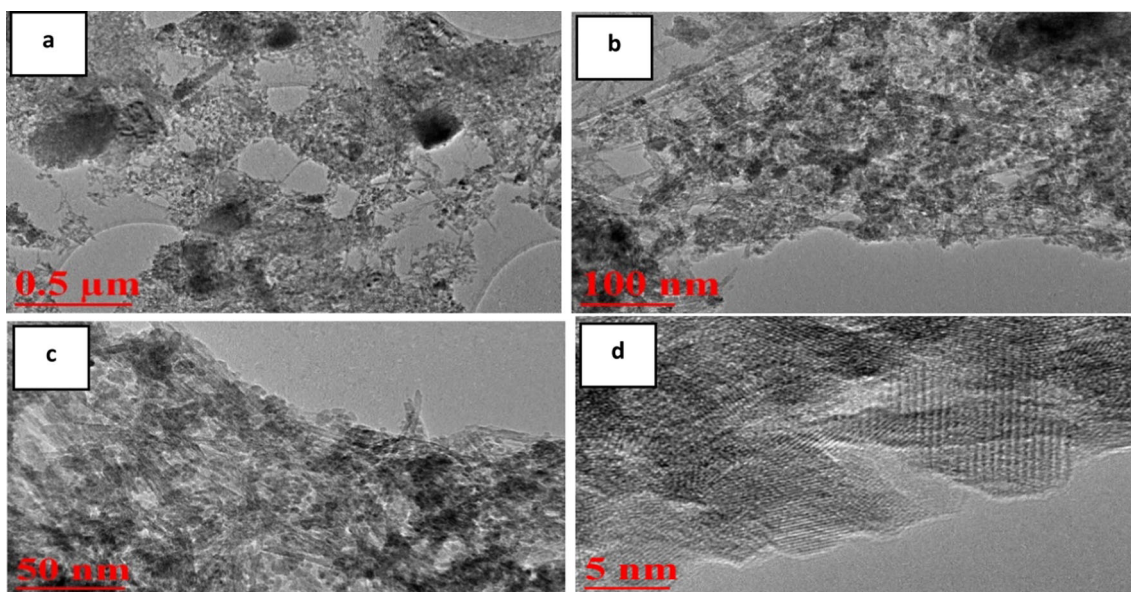


Fig. 5 TEM micrographs of [Cu (INA)₂]-MOF sample with magnification of **a** 10 k, **b** 40 k, **c** 100 k, and **d** 800 k

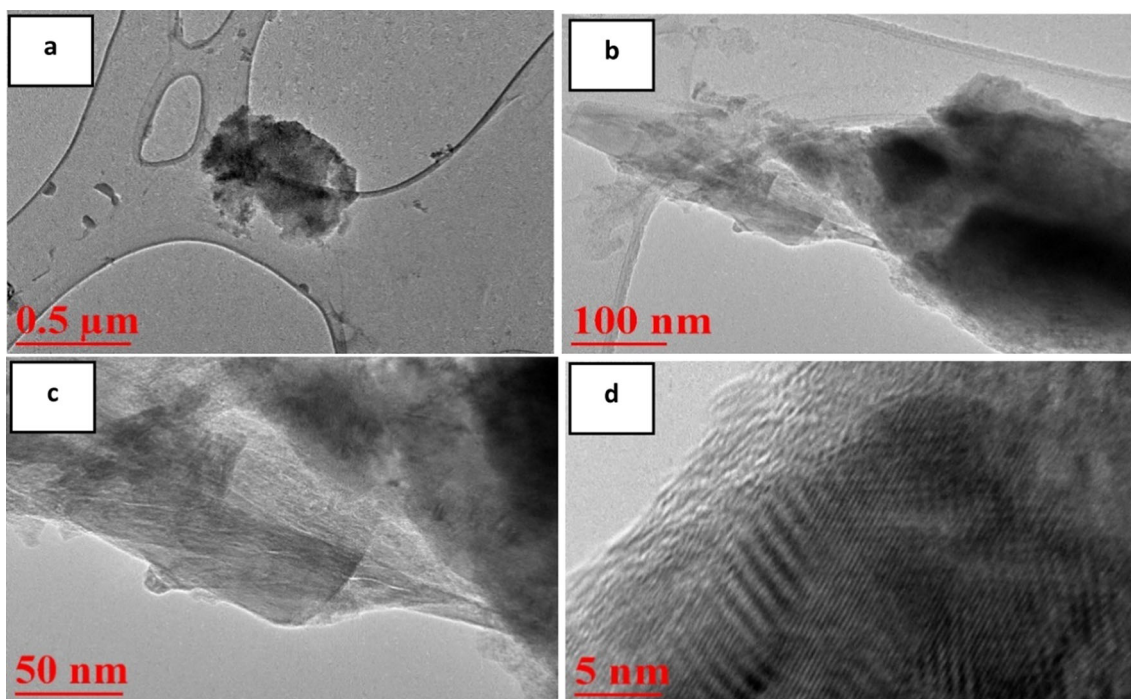


Fig. 6 TEM micrographs of Fe₃O₄-MNPs sample with magnification of **a** 10 k, **b** 40 k, **c** 100 k, and **d** 800 k

The magnification of the [Cu (INA)₂]-MOF@Fe₃O₄ is shown in Fig. 7a, b, c, and d, and the [Cu (INA)₂]-MOF and Fe₃O₄-MNPs were attached to one another and stacked to create multiple channels, and these agglomeration phenomena supplied additional adsorption sites for [Cu (INA)₂]-MOF at Fe₃O₄. The particle size of the synthesized Fe₃O₄-MNPs was bigger than that of the [Cu (INA)₂]-MOF

material, allowing these two components to be distinguished. As a result, the TEM image of [Cu (INA)₂]-MOF@Fe₃O₄ reveals that the structure of Cu (INA)₂-MOF is unaltered following chemical alteration. The TEM picture has given the necessary link between MOF bulk/local structure and composition and their properties. The size of the prepared [Cu

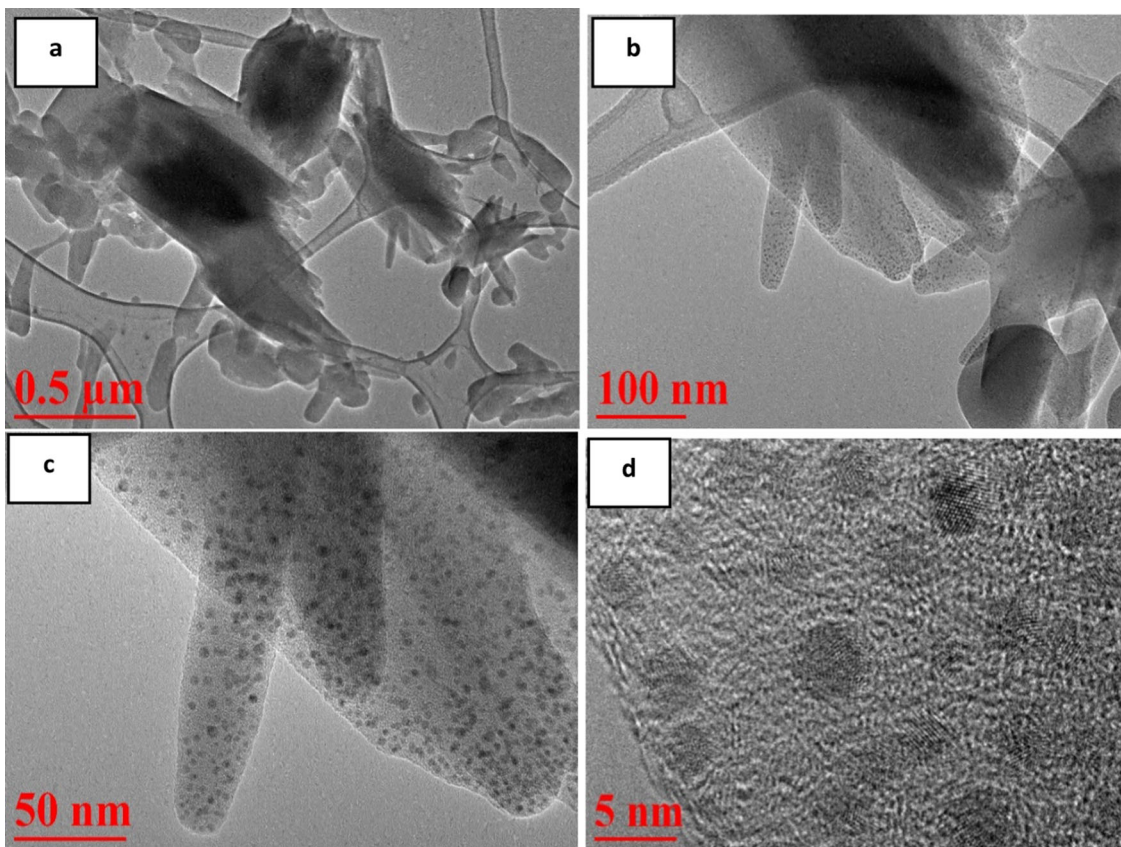


Fig. 7 TEM micrographs of [Cu (INA)₂]-MOF@Fe₃O₄ sample with magnification of **a** 10 k, **b** 40 k, **c** 100 k, and **d** 800 k

(INA)₂-MOF@Fe₃O₄ is more significant (50–100 nm) with multifaceted cuboid particles with rough surfaces.

The XRD used to evaluate the crystallinity properties of the [Cu (INA)₂]-MOF revealed high-intensity peaks in the spectrum at angles 2θ 10.76 and 22.5, with hkl of 100 and 200 acquired (Fig. 8a), and they corresponded with the XRD pattern previously described for the [Cu (INA)₂]-MOF produced by the mechanochemical method [42, 43]. The Scherrer equation is used to calculate the diameters of the sub-micrometer crystallites that make up the peak in a diffraction pattern (Eq. 18) [44–46].

$$D = 1 + \frac{K\lambda}{\beta \cos^2} \tag{18}$$

where *D* is the average size of the ordered (crystalline) domains, *K* is a dimensionless shape factor, λ is the wavelength, β is the line broadening at half the maximum intensity (FWHM), and θ is the Bragg constant, the crystallites size of the MOF was calculated to be 39.78 nm.

The powder X-ray diffraction (PXRD) patterns of Fe₃O₄-MNPs and [Cu (INA)₂]-MOF@Fe₃O₄ are displayed in Fig. 8b and c, respectively. Wide peaks in the diffractogram of the MNPs PXRD pattern indicate that the crystallites are nanometric in size. The sharp and strong diffraction

Table 1 EDX of elemental presentation of the copper isonicotinate [Cu (INA)₂]-MOF

Serial number	Elements	Weight%
1	Carbon	49.8
2	Copper	21.3
3	Oxygen	21.7
4	Nitrogen	7.2
Total		100

peaks indicated the purity and high degree of the crystallization of all the synthesized materials [47]. Magnetite, Fe₃O₄, cannot be ruled out completely, although the pattern matches the cubic symmetry of maghemite, Fe₂O₃, quite well (PDF card 39-1346). When exposed to oxygen, nanoparticles of magnetite are unstable and can transform into maghemite. Magnetite and maghemite are difficult to distinguish through X-ray diffraction due to their identical cell dimensions and shared spinel crystal structure. Table 1 shows the specifics of each value for the EDX elemental analysis from Cu (INA)₂-MOF@Fe₃O₄. The XRD patterns of composite Cu (INA)₂-MOF@Fe₃O₄ and Fe₃O₄-MNPs revealed six distinct peaks for each material. The hkl indices

Fig. 8 XRD pattern of **a** Cu (INA)₂]–MOF, **b** Fe₃O₄–MNPs, and **c** Cu (INA)₂]–MOF @Fe₃O₄

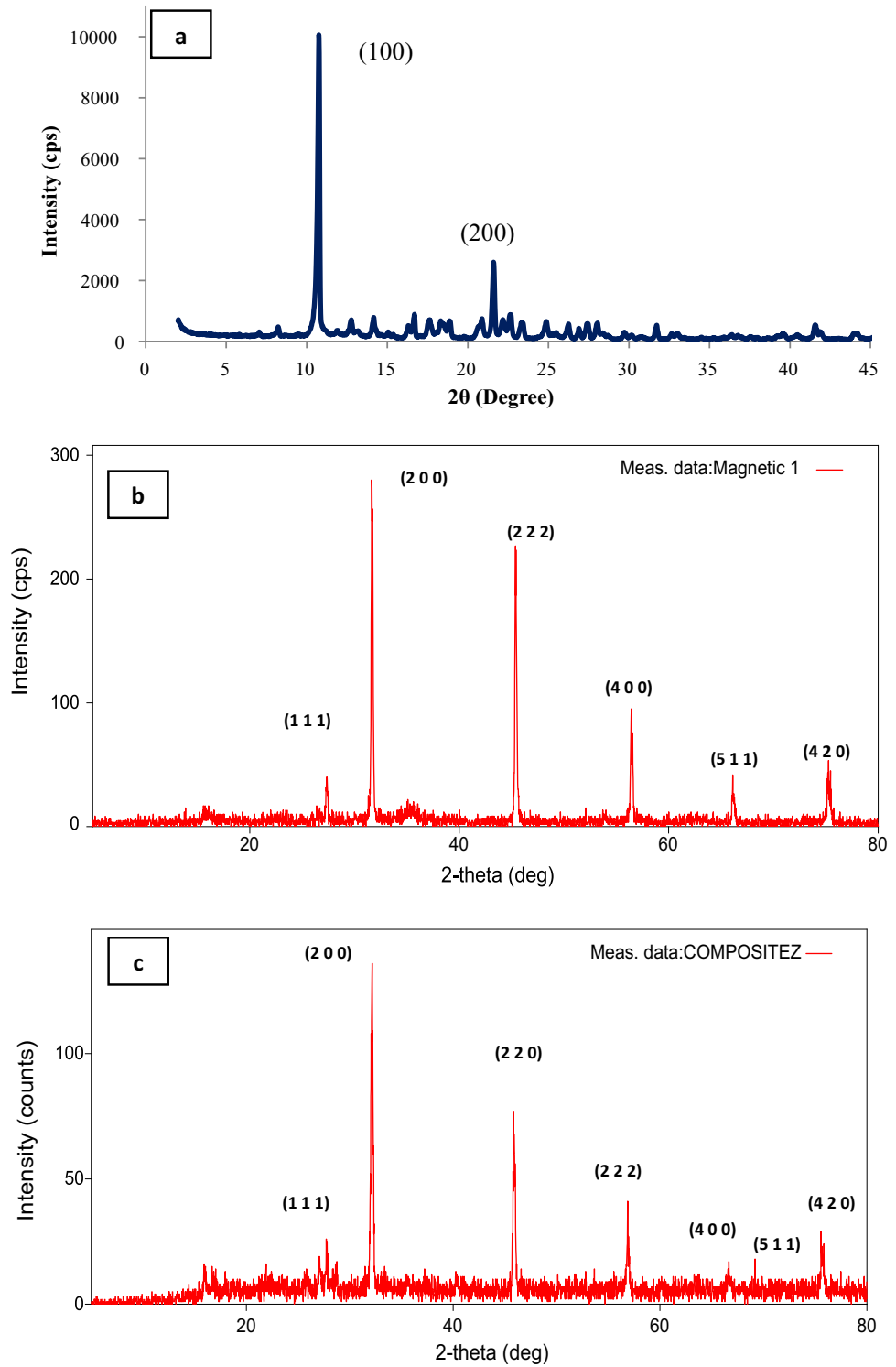




Fig. 9 Synthesized Fe_3O_4 -MNPs tested with laboratory magnet

obtained for the peaks are (1 1 1), (2 0 0), (2 2 0), (4 0 0), and (5 1 1), and an additional peak at (4 2 0) is observed for the $[\text{Cu}(\text{INA})_2]\text{-MOF@Fe}_3\text{O}_4$, indicating the presence of an additional compound. They were observed in both samples, demonstrating that the synthesized nanoparticles were composed entirely of Fe_3O_4 . According to Duan [48], functionalization of a MOF would not have a significant effect on the XRD patterns that could result in a significant change. Using the mechanochemical process [49], nanoparticles with a spinel magnetite crystal structure were produced based on the results. According to a study by Bellusci [22], the crystallinity of magnetic nanoparticles synthesized via a mechanochemical method is superior to other methods, such as coprecipitation under ultrasonication. The tiny size of the crystallites is likely responsible for the larger and overlapping peak profiles observed in the XRD profile when compared to conventional materials. $[\text{Cu}(\text{INA})_2]\text{-MOF@Fe}_3\text{O}_4$'s diffraction profile reveals iron oxide nanoparticle and Fe_3O_4 peaks. Clear and the absence of impurity peaks indicate that the magnetic composite was successfully synthesized. The magnetic force of the composite and the iron oxide materials synthesized in the laboratory were further tested using a permanent magnet in the laboratory (Fig. 9).

Brunauer–Emmet–Teller (BET) surface areas and porosity of the virgin $[\text{Cu}(\text{INA})_2]\text{-MOF}$, magnetic iron oxide nanoparticle (Fe_3O_4), and Cu-based magnetic iron nanoparticle composite-MOF $[\text{Cu}(\text{INA})_2]\text{-MOF@Fe}_3\text{O}_4$ were determined through liquid nitrogen N_2 adsorption tests. The SBET results obtained were good for the adsorption of micropollutants such as β -agonists. The SBET for result for Fe_3O_4 -MNPs measured is $25.3 \text{ m}^2/\text{g}$, whereas the SBET for $(\text{Cu}(\text{INA})_2)\text{-MOF@Fe}_3\text{O}_4$ is $27.2 \text{ m}^2/\text{g}$ which is a great improvement from the measured BET values of $20.4 \text{ m}^2/\text{g}$ obtained for the $([\text{Cu}(\text{INA})_2]\text{-MOF})$ and the results are in compliant with the XRD results and corresponds to an equivalent diameter size of approximately 4 nm. Our new synthesized

adsorbent has a greater surface area than the Fe_3O_4 and their composites that were synthesized by Aryee [50] with $0.29 \text{ m}^2/\text{g}$, $0.40 \text{ m}^2/\text{g}$, and $10.45 \text{ m}^2/\text{g}$, respectively.

3.2 Removal Studies

3.2.1 Effect of Contact Time

It is necessary to understand the influence of contact time duration on adsorption studies to have a thorough knowledge of the equilibrium state in the study. Adsorbate (salbutamol) concentrations of 10, 20, 30, 40, 50 to 60 mg/L were studied, with both the adsorbents (i.e., $[\text{Cu}(\text{INA})_2]\text{-MOF}$ and the $[\text{Cu}(\text{INA})_2]\text{-MOF@Fe}_3\text{O}_4$) doses from 1, 2, 3, 4, 5 to 6 mg/g in the whole research for 1 h and 10 min. Optimum parameters were chosen in both the adsorption studies in both the adsorbents, adsorbate initial concentration of 40 mg/L at pH 11, with a lowest dosages of 1 mg at of 25°C being chosen, the adsorption of salbutamol onto both the $[\text{Cu}(\text{INA})_2]\text{-MOF}$ and $([\text{Cu}(\text{INA})_2]\text{-MOF@Fe}_3\text{O}_4)$ was examined to have a very good adsorption capacity at 40 min contact time. Figure 10 depicts the influence of contact time on the elimination of salbutamol from both the $[\text{Cu}(\text{INA})_2]\text{-MOF}$ and $[\text{Cu}(\text{INA})_2]\text{-MOF@Fe}_3\text{O}_4$. The result revealed that the adsorbate (salbutamol) has an effective % removal of 90.6 and 99.5% from the $[\text{Cu}(\text{INA})_2]\text{-MOF}$ and $[\text{Cu}(\text{INA})_2]\text{-MOF@Fe}_3\text{O}_4$, respectively, and a very good capacity of 1449 and 1592.756 mg/g for $[\text{Cu}(\text{INA})_2]\text{-MOF}$ and $[\text{Cu}(\text{INA})_2]\text{-MOF@Fe}_3\text{O}_4$, respectively. Equilibrium is achieved in a considerable time (40 min) than was previously reported using other adsorbents. Previous studies reported a high contact time of 48 h [18] using micro-grain activated carbon and another reported a contact time of up to 8 weeks [15] using activated carbon as an adsorbent. Our studies indicated more favorable interactions between the salbutamol molecules and the $[\text{Cu}(\text{INA})_2]\text{-MOF@Fe}_3\text{O}_4$ which resulted in having a higher adsorption capacity and greater percent removal than with the $[\text{Cu}(\text{INA})_2]\text{-MOF}$. Faster removal of the pollutant was also observed in the studies better than previously reported adsorbents as reported in Table 4. The same scenario was reported in Saruchi research [38]. The adsorption time was subsequently increased to 70 min to ensure that the $([\text{Cu}(\text{INA})_2]\text{-MOF}$ and the $[\text{Cu}(\text{INA})_2]\text{-MOF@Fe}_3\text{O}_4)$ were effective under the equilibrium condition of the experiment.

3.2.2 Effect of Adsorbate (Salbutamol) Initial Concentration

An investigation of the effect of salbutamol initial concentrations ranging from 10, 20, 30, 40, 50 to 60 mg/L was carried out using the individual adsorbent's dosages ranging from 1, 2, 3, 4, 5 to 6 mg/g. Figure 11 depicts how

Fig. 10 Effect of contact time at adsorbent dosage of 1 mg/g with adsorbate concentrations of 40 mg/L under an alkaline pH of 11 and 25 °C

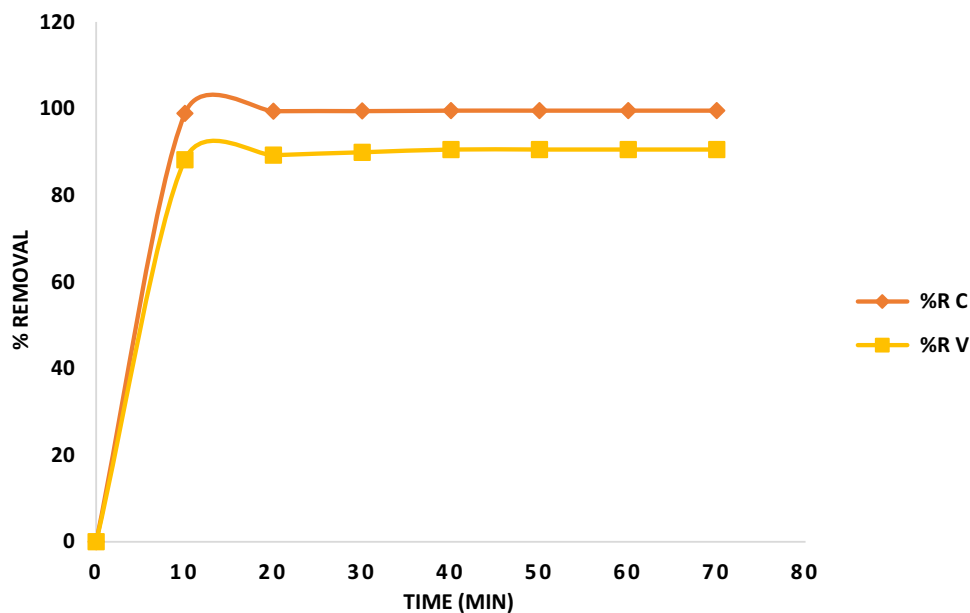
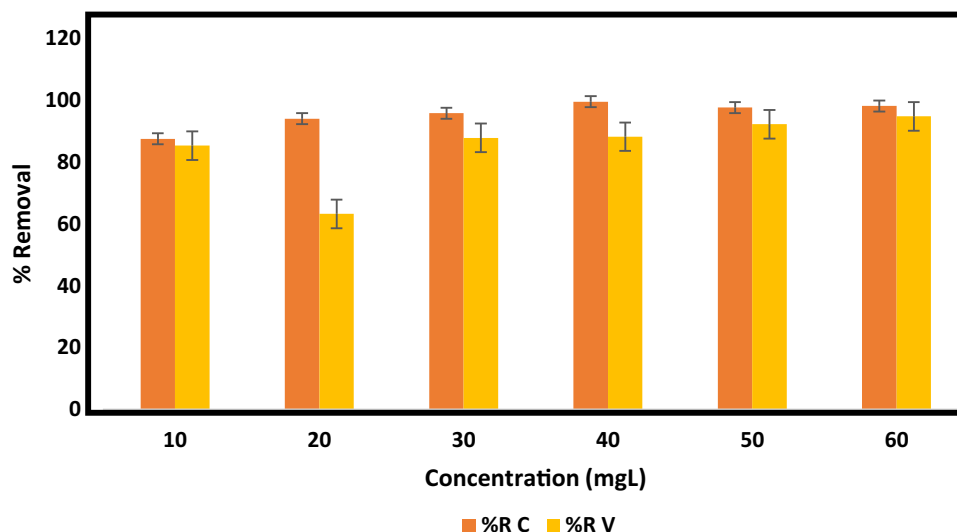


Fig. 11 Effect of adsorbate (Salbutamol) initial concentration at adsorbent dosage of 1 mg/g under 40 min of contact time under an alkaline pH of 11 and 25 °C



the initial concentration of salbutamol affected the adsorption phenomenon by increasing the adsorption capacity as the salbutamol concentrations were subsequently raised. This happened by varying initial concentrations of salbutamol thereby increasing the adsorption capacity. As the concentration of salbutamol in the solution was increased, the active sites of the individual adsorbents ($[\text{Cu}(\text{INA})_2]\text{-MOF}$ and $[\text{Cu}(\text{INA})_2]\text{-MOF@Fe}_3\text{O}_4$) were surrounded by a greater number of salbutamol molecules, resulting in greater adsorption efficiency [43]. The result indicated that even at high salbutamol concentrations, there were still unoccupied adsorption sites that were to be occupied and ready to be occupied as the salbutamol concentration increased. Similar circumstance was obtained by Tella [43].

Our studies considered a 40 mg/L salbutamol initial concentration with an effective removal of 88.2 and 99.5% for the $[\text{Cu}(\text{INA})_2]\text{-MOF}$ and $[\text{Cu}(\text{INA})_2]\text{-MOF@Fe}_3\text{O}_4$, respectively, and a high value of adsorption capacity of 1411.203 and 1592.756 mg/L for the $[\text{Cu}(\text{INA})_2]\text{-MOF}$ and $[\text{Cu}(\text{INA})_2]\text{-MOF@Fe}_3\text{O}_4$, respectively. This unique and excellent value of adsorption capacity from both the adsorbents is an indication of their effectiveness and the better adsorption capacity of the adsorbents, i.e., $[\text{Cu}(\text{INA})_2]\text{-MOF}$ and the $[\text{Cu}(\text{INA})_2]\text{-MOF@Fe}_3\text{O}_4$ in the removal study of salbutamol, with the $[\text{Cu}(\text{INA})_2]\text{-MOF@Fe}_3\text{O}_4$ achieving both higher adsorption capacity and efficiencies than the $[\text{Cu}(\text{INA})_2]\text{-MOF}$ which can be attributed by the magnetic improvement that was coupled with the addition of more OH group and

an increased porosity and vacant sites meted by the magnetic enhancement of the $[\text{Cu}(\text{INA})_2]\text{-MOF@Fe}_3\text{O}_4$ as indicated by the BET results. A previous salbutamol study obtained values around 142 mg/L with 78% removal [18]. On the other hand, tang [51] studied clenbuterol (a β -agonist) and obtained an adsorption capacity of 2.18 mg/L with 81.7% removal.

3.2.3 Effect of Adsorbent Dosage

Adsorbent materials must be capable of achieving maximal adsorption effectiveness even at the lowest feasible dose and in the shortest possible time to be regarded as effective [52]. The study was prepared to investigate the influence of the two adsorbents' dosage ($[\text{Cu}(\text{INA})\text{-MOF}$ and the $[\text{Cu}(\text{INA})_2]\text{-MOF@Fe}_3\text{O}_4$) on salbutamol adsorption. By adjusting the adsorbents' dosages, the estimated quantity of adsorbent dosage that can best remove the contaminants from water can be obtained. The adsorbent dosages were varied between 1, 2, 3, 4, 5 and 6 mg/g in a 40 mL solution with an adsorbate concentrations range of 10, 20, 30, 40, 50 to 60 mg/L, under at alkaline pH of 11 at 25 °C. This study revealed the quantity of salbutamol adsorbed onto the individual adsorbents ($[\text{Cu}(\text{INA})_2]\text{-MOF}$ and the $[\text{Cu}(\text{INA})_2]\text{-MOF@Fe}_3\text{O}_4$) varied with the dose of the adsorbents, as shown in Fig. 12. Adsorption removal effectiveness 90.5 and 99.5 with a good removal capacity of 1449.07 and 1592.75 mg/g were obtained in the overall optimization of adsorbents dosages of $[\text{Cu}(\text{INA})_2]\text{-MOF}$ and the $[\text{Cu}(\text{INA})_2]\text{-MOF@Fe}_3\text{O}_4$ at the lowest dosage of 1 mg/g. The study considered the lowest adsorbent dosage of 1 mg/g under 40 min of contact time with adsorbate concentrations of 40 mg/L under an alkaline pH of 11 and 25 °C in this study. Previous research by Wang [53] obtained similar findings to our study.

3.2.4 Effect of pH

For a successful adsorption experimental study between these compounds, pH should play a major influence considering the pK_a of the adsorbents (4–5) and the adsorbate (9.72). To understand the pH influence on salbutamol adsorption onto the ($[\text{Cu}(\text{INA})_2]\text{-MOFs}$ and the $[\text{Cu}(\text{INA})_2]\text{-MOF@Fe}_3\text{O}_4$, various pH values (3, 5, 7, 9, 11, and 13) were studied, because the pH of the solution has a very strong impact on aqueous phase adsorptions. As demonstrated in Fig. 13 adsorption of salbutamol is greatly influenced by the pH of the solution as the state of the salbutamol (adsorbates) either in protonated, neutral, or deprotonated forms, as well as the adsorbents, as the surface charge of ($[\text{Cu}(\text{INA})\text{-MOF}$ and the $[\text{Cu}(\text{INA})_2]\text{-MOF@Fe}_3\text{O}_4$ is significantly influenced by the pH of the solution in which they are deposited [54].

The studies shows that the pH of the solution has direct proportionality relation with the adsorption effectiveness (demonstrated in Fig. 13); thereby, as the pH of the solution is increased the adsorption effectiveness increased up to pH 11 with a very high percentage removal of 97.23 and 97.69% for the $[\text{Cu}(\text{INA})_2]\text{-MOF}$ and the $[\text{Cu}(\text{INA})_2]\text{-MOF@Fe}_3\text{O}_4$, respectively, indicating that these phenomena (pH 11) favor the adsorption process of both the adsorbents [19]. A sequential elevation in solution pH bring a significant increase in adsorption capacity due to the attraction between the negatively charged adsorbent surface (previous zeta potential study) and the salbutamol's positive charged molecule.

3.2.5 Adsorption Isotherm Study

The findings obtained for all parameters in the isotherm models that include R^2 , RMSE, and AIC were more satisfying and most fitted to the Langmuir model than the values obtained for the other models studied in both the ($[\text{Cu}(\text{INA})_2]\text{-MOF}$ and the $[\text{Cu}(\text{INA})_2]\text{-MOF@Fe}_3\text{O}_4$, as indicated in Table 2, and the graphical representations of these results are provided in the supplementary Figures a, b, and c. The RL values produced for both the materials, on the other hand, were less than unity 0.81 and 0.71 for the ($[\text{Cu}(\text{INA})\text{-MOF}$ and the $[\text{Cu}(\text{INA})_2]\text{-MOF@Fe}_3\text{O}_4$, respectively, indicating that the method was successful and that both the ($[\text{Cu}(\text{INA})_2]\text{-MOFs}$ and the $[\text{Cu}(\text{INA})_2]\text{-MOF@Fe}_3\text{O}_4$ materials maintained monolayer interactions with the salbutamol molecules throughout the experiment. Therefore, it was revealed that both the $[\text{Cu}(\text{INA})_2]\text{-MOF}$ and the modified $[\text{Cu}(\text{INA})_2]\text{-MOF@Fe}_3\text{O}_4$ synthesized and used in our laboratory had homogenous adsorption sites, which resulted in increased adsorption of the analyte (Salbutamol) in both the materials. Similar findings have been published in Zango's most recent papers [55, 56]. Moreover, the synthesized $[\text{Cu}(\text{INA})_2]\text{-MOF@Fe}_3\text{O}_4$ obtained in our laboratory shows better performance in all the required parameters by comparing the results from both the adsorbents with lower AIC, RMSE, and RL values.

3.2.6 Adsorption Kinetics Study

Salbutamol adsorption on all the as-synthesized adsorbents, i.e., $[\text{Cu}(\text{INA})_2]\text{-MOF}$ and $[\text{Cu}(\text{INA})_2]\text{-MOF@Fe}_3\text{O}_4$, are both dependent on the interaction between the adsorbate and their surfaces, which all have both donor and acceptor functional sites (OH, N). The kinetics of the adsorption process as a function of adsorbent dose were therefore calculated using the pseudo-first-order, pseudo-second-order, and intraparticle diffusion models. Better fitting of R^2 adjusted R^2 , RMSE, and smaller AIC values was used to define the models. According to the statistical values displayed in Table 3, the pseudo-second-order model has the best fitting support for

Fig. 12 Effect of adsorbent Dosage under 40 min of contact time with adsorbate concentrations of 40 mg/L under an alkaline pH of 11 and 25 °C

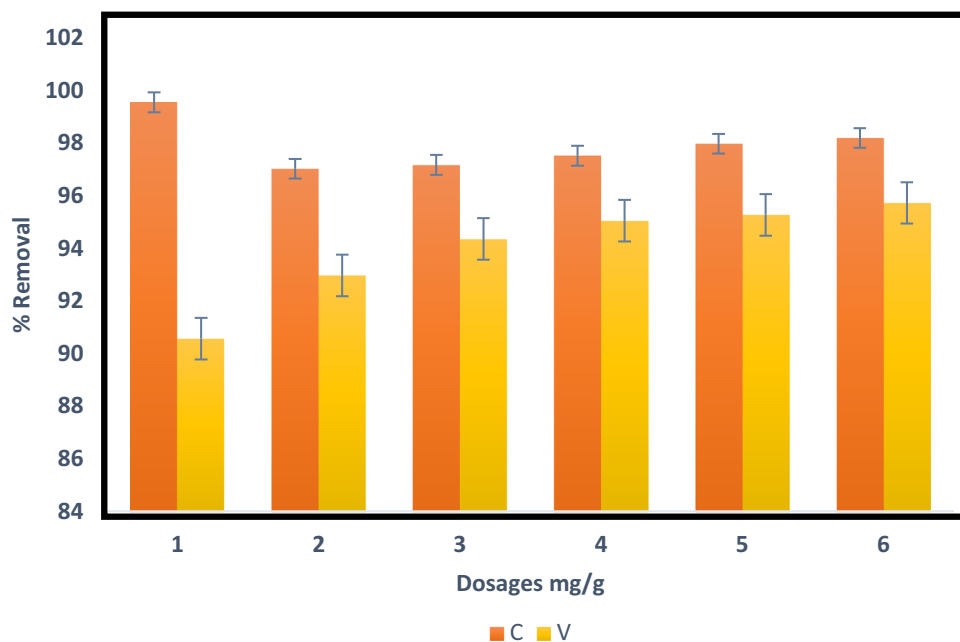
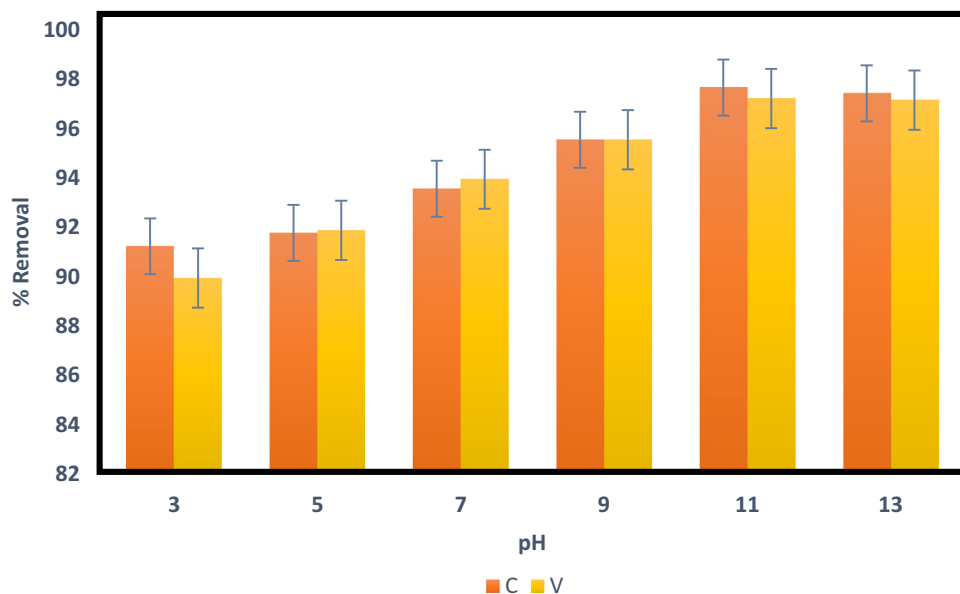


Fig. 13 pH Effect on the adsorbents at adsorbent dosage of 1 mg/g under 40 min of contact time with adsorbate concentrations of 40 mg/L and 25 °C



the majority of the adsorption data in the two applied adsorbents. Furthermore, the observed q_e (mg/g) values match the experimental results in all the adsorbents. The outcome was consistent with Hamza's findings [37, 57, 58].

3.3 Adsorption Mechanism

Through the process of H-bonding, MOFs can generally interact with pharmaceuticals in two different ways: either as H-donors or also as H-acceptors. So, considering the studied interactions in our adsorption the $-OH$ groups in both the $[Cu(INA)-MOF]$ and the $[Cu(INA)_2]-MOF@Fe_3O_4$ and the salbutamol are rather stable, and the state of both may

be assessed to better understand the mechanisms. They both have a highly polar hydrogen atom attached to each of their nitrogen and oxygen atoms that they are both H-donors. In addition, both the nitrogen and oxygen atoms bound to hydrogen have an identical partial negative charge capable of accepting H-bonds because they both possess lone electron pairs and therefore act as H-acceptor [59, 60]. And these bonds are formed as a result of a considerable electron density deficiency within the donor group or an excess of electrons in the acceptor group.

Given that salbutamol is a tertiary amine with an acidity constant (pK_a) of 9.86 and a considerable number of

Table 2 Isotherm parameters for adsorption of salbutamol onto the [Cu (INA)₂]-MOFs and [Cu (INA)₂]-MOF@Fe₃O₄

Isotherms models	Parameters	[Cu (INA) ₂]-MOF	[Cu (INA) ₂]-MOF@Fe ₃ O ₄
Langmuir	q_m (mg/g)	1440	2000
	K_L (L/mg)	0.006	0.01
	R_L	0.81	0.71
	R^2	0.9969	0.9988
	R^2_{adj}	0.877	0.121
	RMSE	0.011	0.017
	AIC	- 52.946	- 55.546
Freundlich	K_F (L/g)	1.065	1.295
	N	0.2087	0.0263
	R^2	0.9912	0.9616
	R^2_{adj}	0.0287	0.337
	RMSE	0.052	0.012
	AIC	- 39.616	- 60.143
	Temkin	A (L/g)	1.0007
b_T (kJ/mol)		989.06	9908.5
R^2		0.9819	0.9684
R^2_{adj}		0.0287	0.337
RMSE		0.052	0.012
AIC		- 39.616	- 60.144

Table 3 Adsorption kinetics parameters for the removal of Salbutamol the virgin ([Cu (INA)₂]-MOF and the [Cu (INA)₂]-MOF@Fe₃O₄

Kinetics models	Parameters	[Cu (INA) ₂]-MOF	[Cu (INA) ₂]-MOF@Fe ₃ O ₄
Pseudo-first order	q_{exp} (mg/g)	1450	1950.6
	q_{cal} (mg/g)	2.718	2.649
	K_1	0.0674	0.0695
	R^2	0.7714	0.715
	R^2_{adj}	0.594	0.939
	RMSE	1.229	2.460
	AIC	- 6.95	- 6.106
Pseudo-second order	q_{exp} (mg/g)	1440	1950.6
	q_{cal} (mg/g)	256	2000
	K_2 (mg/g min)	1.52	0.05
	R^2	1	1
	R^2_{adj}	0.90	1
	RMSE	0.009	0.007
	AIC	- 121.5	- 68.58
Intraparticle diffusion	K_2 (mg/g min)	0.0014	32.484
	C	1	1139.1
	R^2	1	0.333
	R^2_{adj}	0.080	0.850
	RMSE	0.107	4.189
	AIC	- 29.7	21.70

OH group and N species that are both H-donor and H-acceptor sites [59]. The discovery that –OH groups have a positive effect on the q_t value across a wide variety of situations can be interpreted by the process of H-bonding (our research study also investigated salbutamol in a different range of pH values too) [60]. The q_t values rise when the concentration of salbutamol was increased as illustrated in Fig. 11, and the –OH groups in salbutamol are very stable considering its highly lower acidity. Consequently, the H-bonding mechanism may be explored since the two as-synthesized adsorbents ([Cu (INA)₂]-MOF and the composite [Cu (INA)₂]-MOF@Fe₃O₄) has the potential of acting as both an H-donor and an H-acceptor at the same time as they have the OH groups and N species.

3.4 Effect of Temperature and Thermodynamic

Following the experimental study with the synthesized materials and the analyte, the values of the percentage removal obtained were observed to significantly dropped from 97.23 to 75% for the ([Cu (INA)-MOF and 98.68–75% for the [Cu (INA)₂]-MOF@Fe₃O₄ (Fig. 14), indicating that the process is endothermic. Furthermore, the values of all the thermodynamic parameters were negative and decreased as the temperatures increased as indicated in Table 4 while the values of ΔH° in the ([Cu (INA)₂]-MOF (1.033) and the [Cu (INA)₂]-MOF@Fe₃O₄ (0.053) are all positive, likewise all the values ΔS° obtained 0.127 and 0.00651 were positive too. In addition, these findings demonstrated that the process is spontaneously taking place at random and that the adsorption of salbutamol on the [Cu (INA)₂]-MOF and the [Cu (INA)₂]-MOF@Fe₃O₄ were unfavorable at elevated temperatures.

3.5 Reusability and Regeneration

The ease with which an adsorbent could be recovered and successively reused following active batch adsorption studies highlights their promise as an adsorbent for adsorbate removal from solution.

After active batch adsorption experiments with our [Cu (INA)-MOF and the [Cu (INA)₂]-MOF@Fe₃O₄ were recovered and reused demonstrating the promise of these materials as adsorbents for the removal of salbutamol from the solution. Notably, even after the fifth usage, it can be observed from Fig. 15 that the percent removal accomplished in all the cycles was highly efficient. With more than 97 percent removal efficiency, the [Cu (INA)-MOF and the [Cu (INA)₂]-MOF@Fe₃O₄ used as adsorbent showed a thorough reusability in this application.

3.6 Comparison Studies

An investigation was conducted to determine the efficacy of the currently examined adsorbent material with other accessible previously reported adsorbent materials on the adsorption of salbutamol in water. As shown in Table 4, salbutamol studies and even β -agonists, in general, are understudied, and as a result, no reported study on salbutamol's adsorption using recent materials (including [Cu (INA)-MOF and the magnetic [Cu (INA)₂]-MOF@Fe₃O₄) has been found by the author. Therefore, we consider the very limited studied options (available to us) on adsorption of salbutamol in water using other adsorbents such as granular activated carbon [18], micro-grain activated carbon [18], and, succinylated cellulose nanofibrils (CNFs) even though not enough relevant parameters were available for full comparison. Table 5 considers four parameters that are the determinant factor (in every result of adsorption), and their values are considered an important outcome of the adsorption studies for the best result to be chosen. These determinant factors are (1) adsorbent material, (2) equilibrium time, (3) Q_{max} , and (4) the percentage removal of the analyte. Observation from the table shows that some studies are lacking in one or two parameters that give our study an advantage in the comparison, while great differences were observed in some studied parameters.

4 Conclusion

Following the successful mechano-synthesis of copper isonicotinate metal–organic frameworks ([Cu (INA)₂]-MOF and subsequent synthesis of Fe₃O₄-MNPs, we were able to successfully functionalized the two to obtain the magnetic composite-MOF ([Cu (INA)₂]-MOF@Fe₃O₄) using mortar and pestle. The products were also characterized to by FTIR analysis that revealed the presence of active functional groups and TG analysis that confirmed a strong thermal stability of the framework on temperatures above 250 °C. The XRD spectra also revealed aspects of the [Cu (INA)₂]-MOF and the [Cu (INA)₂]-MOF@Fe₃O₄ crystallinity with an additional peak for the [Cu (INA)₂]-MOF@Fe₃O₄ confirming the additional compound present in the material. The SEM and TEM results show the apparent morphological electronic features of the three materials. Great improvement from the measured BET values was observed for (Cu (INA)₂MOFs@Fe₃O₄) with 27.2 m²/g from the values of 20.4 m²/g obtained for the [Cu (INA)-MOF and the results are in compliant with the XRD results and correspond to an equivalent diameter size of approximately 4 nm.

The pseudo-second-order kinetic model and Langmuir's isotherm model were the best fit models based on statistical fits of R^2 , RMSE, and AIC in all the adsorbents. We were able to achieve a good removal capacity of salbutamol

Fig. 14 Effect of temperature on the adsorption of salbutamol on [Cu (INA)₂]-MOF and [Cu (INA)₂]-MOF@Fe₃O₄

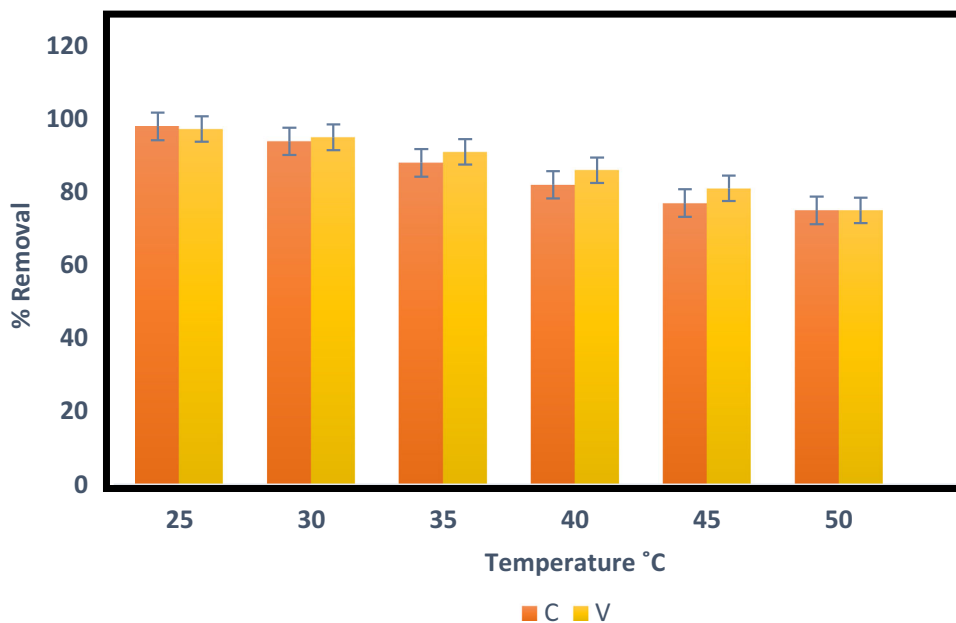


Table 4 Thermodynamic parameters for the adsorption of salbutamol onto [Cu (INA)₂]-MOF# and [Cu (INA)₂]-MOF@Fe₃O₄*

Temp. (K)	$\Delta G^{\circ\#}$ (kJ/mol)	$\Delta G^{\circ*}$ (kJ/mol)	ΔH° (KJ/mol)	ΔS° (J/mol K)
298	-0.0368	-0.00189	0.053*	
303	-0.0374	-0.00192	1.033#	
308	-0.0381	-0.00195		0.00651*
313	-0.0387	-0.00198		0.127#
318	-0.0394	-0.00202		
323	-0.0399	-0.00205		

Fig. 15 Adsorbents reusability

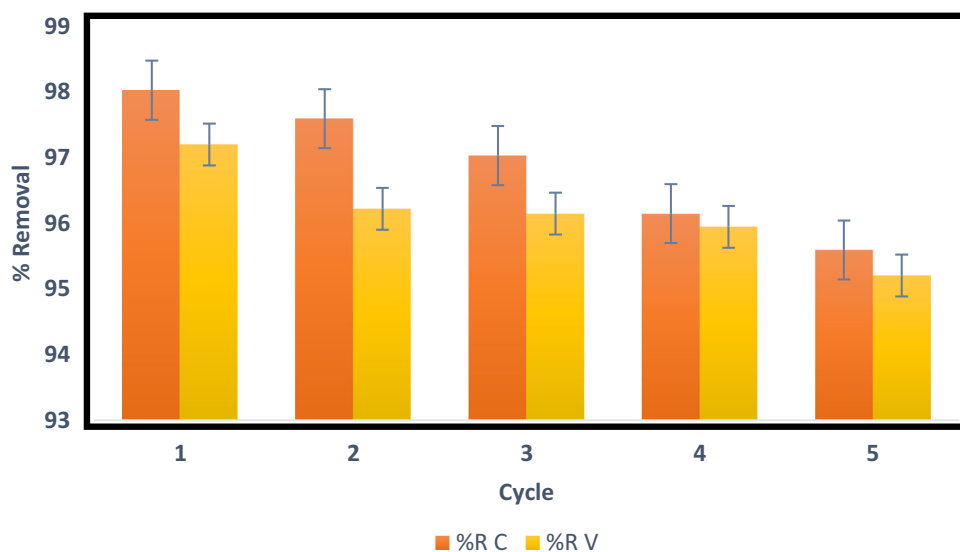


Table 5 Adsorbents reported for the removal of salbutamol from water in comparison with the present study

Adsorbent materials	Equilibrium time	Q_{\max} (mg/g)	% Removal	Analytes	References
μ -Grain activated carbon	48 h	142	78.6	Salbutamol	[18]
Granular activated carbon	8 weeks	N.A.	83.0	Salbutamol	[15]
Succinylated cellulose nanofibrils (CNFs)	30 min	196	20	Salbutamol	[19]
Electronegative silanized β -Cyclodextrin	30 min	140	76	Salbutamol	[61]
Al(III)-MOF (BUT-19)	35 min	366	51	Ractopamine	[62]
Al(III)-MOF (BUT-19)	35	294	52	Clenbuterol	[62]
Ui-66 MOF	60	160	80	Clenbuterol	[27]
[Cu (INA) ₂]-MOF	40 min	1450	97	Salbutamol	This study
[Cu (INA) ₂]-MOF@Fe ₃ O ₄	40 min	2000	98	Salbutamol	This study

within 40 min using the lowest dose of 1 mg/g of all the adsorbent with a Q_{\max} of 1450 for [Cu (INA)-MOF and an improved 2000 mg/g for [Cu (INA)₂]-MOF@Fe₃O₄ which can be related to the iron oxide functionalization. As a consequence of our research, the ([Cu (INA)₂]-MOF and the [Cu (INA)₂]-MOF@Fe₃O₄ have both shown remarkable performances in salbutamol adsorption from environmental water with [Cu (INA)₂]-MOF@Fe₃O₄ having more advantages in all aspects including lower AIC, RSME and RL value and higher R^2 , adjusted R^2 adsorption capacity and adsorption efficiency over the [Cu (INA)₂]-MOF due to the modification that enhances its adsorption capabilities and its thus suggested for use in water remediation and removal of salbutamol and other β -agonists in our environment.

Supplementary Information The online version contains supplementary material available at <https://doi.org/10.1007/s13369-023-08167-z>.

Acknowledgements The authors would like to thank University Malaysia Terengganu (UMT), Postgraduate Research Grant (PG-RG Vot: 55202), Faculty of Science and Marine Environment for the facilities provided throughout this study. The authors would also like to thank the Centre for Functional Materials and Nanotechnology, Institute of Science, Universiti Teknologi MARA, Shah Alam, Malaysia, for their support in completing this work.

References

1. Armayau, U.; Ariffin, M.M.; Loh, S.H.; Mohd Khalik, W.M.A.W.; Yusoff, H.M.: β -Agonist in the environmental waters: a review on threats and determination methods. *Green Chem. Lett. Rev.* **15**(1), 232–251 (2022). <https://doi.org/10.1080/17518253.2022.2032843>
2. Yan, K., et al.: Rapid screening of toxic salbutamol, ractopamine, and clenbuterol in pork sample by high-performance liquid chromatography—UV method. *J. Food Drug Anal.* **24**(2), 277–283 (2016). <https://doi.org/10.1016/j.jfda.2015.12.002>
3. Sakai, N.; Sakai, M.; Mohamad Haron, D.E.; Yoneda, M.; Ali Mohd, M.: Beta-agonist residues in cattle, chicken and swine livers at the wet market and the environmental impacts of wastewater from livestock farms in Selangor State, Malaysia. *Chemosphere* **165**, 183–190 (2016). <https://doi.org/10.1016/j.chemosphere.2016.09.022>
4. Gu, C.; Ren, P.; Zhang, F.; Zhao, G.; Shen, J.; Zhao, B.: Detection of six β -agonists by three multiresidue immunosensors based on an anti-bovine serum albumin-ractopamine-clenbuterol-salbutamol antibody. *ACS Appl. Mater. Interfaces* (2020). <https://doi.org/10.1021/acsomega.0c00249>
5. Lust, E.B.; Barthold, C.; Malesker, M.A.; Wichman, T.O.: Human health hazards of veterinary medications: information for emergency departments. *J. Emerg. Med.* **40**(2), 198–207 (2011). <https://doi.org/10.1016/j.jemermed.2009.09.026>
6. Yan, H.; Xu, D.; Meng, H.; Shi, L.; Li, L.: Food poisoning by clenbuterol in China. *Qual. Assur. Saf. Crop. Foods* **7**(1), 27–35 (2014). <https://doi.org/10.3920/QAS2014.x006>
7. Sakai, N.; Mohd Yusof, R.; Sapar, M.; Yoneda, M.; Ali Mohd, M.: Spatial analysis and source profiling of beta-agonists and sulfonamides in Langat River basin, Malaysia. *Sci. Total Environ.* **548–549**, 43–50 (2016). <https://doi.org/10.1016/j.scitotenv.2016.01.040>
8. Ternes, T.A.: Occurrence of drugs in German sewage treatment plants and rivers. *Water Res.* **32**(11), 3245–3260 (1998). [https://doi.org/10.1016/S0043-1354\(98\)00099-2](https://doi.org/10.1016/S0043-1354(98)00099-2)
9. Dodson, L.G.; Vogt, R.A.; Marks, J.; Reichardt, C.; Crespo-Hernández, C.E.: Photophysical and photochemical properties of the pharmaceutical compound salbutamol in aqueous solutions. *Chemosphere* **83**(11), 1513–1523 (2011). <https://doi.org/10.1016/j.chemosphere.2011.01.048>
10. Yamini, Y.; Reimann, C.T.; Vatanara, A.; Ake, J.; Jönsson, J.Å.: Extraction and preconcentration of salbutamol and terbutaline from aqueous samples using hollow fiber supported liquid membrane containing anionic carrier. *J. Chromatogr. A* **1124**(1–2), 57–67 (2006). <https://doi.org/10.1016/j.chroma.2006.05.001>
11. Yalkowsky, H., He, S.Y., Parijat, J.: Handbook of Aqueous Solubility Data. In: Handbook of aqueous solubility data: an extensive compilation of aqueous solubility data for organic compounds extracted from the AQUASOL database, p. 1620. CRC Press, Boca Raton (2019)
12. Lan, Y.; Coetsier, C.; Causserand, C.; Groenen Serrano, K.: An experimental and modelling study of the electrochemical oxidation of pharmaceuticals using a boron-doped diamond anode. *Chem. Eng. J.* **333**(June 2017), 486–494 (2018). <https://doi.org/10.1016/j.cej.2017.09.164>
13. Lian, L.; Yao, B.; Hou, S.; Fang, J.; Yan, S.; Song, W.: Kinetic study of hydroxyl and sulfate radical-mediated oxidation of pharmaceuticals in wastewater effluents. *Environ. Sci. Technol.* **51**(5), 2954–2962 (2017). <https://doi.org/10.1021/acs.est.6b05536>



14. Yan, S., et al.: Development of fluorescence surrogates to predict the photochemical transformation of pharmaceuticals in wastewater effluents. *Environ. Sci. Technol.* **51**(5), 2738–2747 (2017). <https://doi.org/10.1021/acs.est.6b05251>
15. de Ridder, D.J., et al.: Influence of natural organic matter on equilibrium adsorption of neutral and charged pharmaceuticals onto activated carbon. *Water Sci. Technol.* **63**(3), 416–423 (2011). <https://doi.org/10.2166/wst.2011.237>
16. Sakkas, V.A., et al.: Heterogeneous photocatalytic degradation of the pharmaceutical agent salbutamol in aqueous titanium dioxide suspensions. *Appl. Catal. B Environ.* **77**(1–2), 135–144 (2007). <https://doi.org/10.1016/j.apcatb.2007.07.017>
17. Zango, Z.U., et al.: A critical review on metal-organic frameworks and their composites as advanced materials for adsorption and photocatalytic degradation of emerging organic pollutants from wastewater. *Polymers (Basel)* **12**(11), 2648 (2020). <https://doi.org/10.3390/polym12112648>
18. Alves, T.C.; Cabrera-Codony, A.; Barceló, D.; Rodriguez-Mozaz, S.; Pinheiro, A.; Gonzalez-Olmos, R.: Influencing factors on the removal of pharmaceuticals from water with micro-grain activated carbon. *Water Res.* **144**, 402–412 (2018). <https://doi.org/10.1016/j.watres.2018.07.037>
19. Selkälä, T., et al.: Rapid uptake of pharmaceutical salbutamol from aqueous solutions with anionic cellulose nanofibrils: The importance of pH and colloidal stability in the interaction with ionizable pollutants. *Chem. Eng. J.* **350**, 378–385 (2018). <https://doi.org/10.1016/j.cej.2018.05.163>
20. Abu-Dief, A.M.; Alrashedee, F.M.M.; Emran, K.M.; Al-Abdulkarim, H.A.: Development of some magnetic metal-organic framework nano composites for pharmaceutical applications. *Inorg. Chem. Commun.* (2022). <https://doi.org/10.1016/j.inoche.2022.109251>
21. Mazaj, M.; Kaučič, V.; ZabukovecLogar, N.: Chemistry of metal-organic frameworks monitored by advanced X-ray diffraction and scattering techniques. *Acta Chim. Slov.* **63**(3), 440–458 (2016). <https://doi.org/10.17344/acs.2016.2610>
22. Bellusci, M., et al.: Magnetic metal-organic framework composite by fast and facile mechanochemical process. *Inorg. Chem.* **57**(4), 1806–1814 (2018). <https://doi.org/10.1021/acs.inorgchem.7b02697>
23. Chughtai, A.H.; Ahmad, N.; Younus, H.A.; Laypkov, A.; Verpoort, F.: Metal-organic frameworks: versatile heterogeneous catalysts for efficient catalytic organic transformations. *Chem. Soc. Rev.* **44**(19), 6804–6849 (2015). <https://doi.org/10.1039/c4cs00395k>
24. Tajuddin, M.H.A., et al.: Metal organic framework in membrane separation for wastewater treatment: potential and way forward. *Arab. J. Sci. Eng.* **46**(7), 6109–6130 (2021). <https://doi.org/10.1007/s13369-021-05509-7>
25. Isiyaka, H.A., et al.: Experimental and modeling of dicamba adsorption in aqueous medium using MIL-101(Cr) metal-organic framework. *Processes* **9**(3), 1–18 (2021). <https://doi.org/10.3390/pr9030419>
26. Juan-alcan, J., et al.: Towards acid MOFs—catalytic performance of sulfonic acid functionalized architectures†. *Catal. Sci. Technol.* **101**, 2311–2318 (2013). <https://doi.org/10.1039/c3cy00272a>
27. Yang, H., et al.: Determination and removal of clenbuterol with a stable fluorescent zirconium(IV)-based metal organic framework. *Microchim. Acta* **186**(7), 454 (2019). <https://doi.org/10.1007/s00604-019-3586-3>
28. Zhao, Y., et al.: Metal organic frameworks for energy storage and conversion. *Energy Storage Mater.* **2**(November), 35–62 (2016). <https://doi.org/10.1016/j.ensm.2015.11.005>
29. Chowdhury, M.A.: Metal-organic-frameworks for biomedical applications in drug delivery, and as MRI contrast agents. *J. Biomed. Mater. Res. Part A* **105**(4), 1184–1194 (2017). <https://doi.org/10.1002/jbm.a.35995>
30. Ahmed, I.; Jhung, S.H.: Composites of metal-organic frameworks: preparation and application in adsorption. *Mater. Today* **17**(3), 136–146 (2014). <https://doi.org/10.1016/j.mattod.2014.03.002>
31. Zeng, M.H.; Wang, B.; Wang, X.Y.; Zhang, W.X.; Chen, X.M.; Gao, S.: Chiral magnetic metal-organic frameworks of dimetal sub-units: magnetism tuning by mixed-metal compositions of the solid solutions. *Inorg. Chem.* **45**(18), 7069–7076 (2006). <https://doi.org/10.1021/ic060520g>
32. Tella, A.; Nwosu, F.; Adimula, V.: Removal of anthracene from solution using [Cu (INA)₂] metal-organic frameworks synthesized by a solvent free method. *Niger. J. Mater. Sci. Eng.* **7**, 26 (2016)
33. Bellusci, M., et al.: Manganese iron oxide superparamagnetic powder by mechanochemical processing. Nanoparticles functionalization and dispersion in a nanofluid. *J. Nanoparticle Res.* **14**(6), 1–11 (2012). <https://doi.org/10.1007/s11051-012-0904-7>
34. Jannah, N.R.; Onggo, D.: Synthesis of Fe₃O₄ nanoparticles for colour removal of printing ink solution. *J. Phys. Conf. Ser.* **1245**(1), 012040 (2019). <https://doi.org/10.1088/1742-6596/1245/1/012040>
35. Isiyaka, H.A.; Jumbri, K.; Sambudi, N.S.; Zango, Z.U.; Saad, B.; Mustapha, A.: Removal of 4-chloro-2-methylphenoxyacetic acid from water by MIL-101(Cr) metal-organic framework: kinetics, isotherms and statistical models. *R. Soc. Open Sci.* **8**(1), 201553 (2021). <https://doi.org/10.1098/rsos.201553>
36. Abdel-Rahman, L.H.; Abu-Dief, A.M.; Al-Farhan, B.S.; Yousef, D.; El-Sayed, M.E.A.: Kinetic study of humic acid adsorption onto smectite: the role of individual and blend background electrolyte. *AIMS Mater. Sci.* **6**(6), 1176–1190 (2019). <https://doi.org/10.3934/mat.2019.6.1176>
37. Isiyaka, H.A., et al.: Adsorption of dicamba and MCPA onto MIL-53(Al) metal-organic framework: response surface methodology and artificial neural network model studies. *RSC Adv.* **10**(70), 43213–43224 (2020). <https://doi.org/10.1039/D0RA07969C>
38. Kumar, V.: Adsorption kinetics and isotherms for the removal of rhodamine B dye and Pb+2 ions from aqueous solutions by a hybrid ion-exchanger. *Arab. J. Chem.* **12**(3), 316–329 (2019). <https://doi.org/10.1016/j.arabjc.2016.11.009>
39. Liu, Y.H.; Lu, Y.L.; Tsai, H.L.; Wang, J.C.; Lu, K.L.: Hydrothermal synthesis, crystal structure, and magnetic property of copper(II) coordination networks with chessboard tunnels. *J. Solid State Chem.* **158**(2), 315–319 (2001). <https://doi.org/10.1006/jssc.2001.9118>
40. Chen, Y.; Li, L.; Li, J.; Ouyang, K.; Yang, J.: Ammonia capture and flexible transformation of M-2(INA) (M=Cu Co, Ni, Cd) series materials. *J. Hazard. Mater.* **306**, 340–347 (2016). <https://doi.org/10.1016/j.jhazmat.2015.12.046>
41. Shi, G.; Xu, W.; Wang, J.; Yuan, Y.; Chaemchuen, S.; Verpoort, F.: A Cu-based MOF for the effective carboxylation of terminal alkynes with CO₂ under mild conditions. *J. CO₂ Util.* **39**, 101177 (2020). <https://doi.org/10.1016/j.jcou.2020.101177>
42. Pichon, A.; Lazuen-Garay, A.; James, S.L.: Solvent-free synthesis of a microporous metal-organic framework. *CrystEngComm* **8**(3), 211–214 (2006). <https://doi.org/10.1039/b513750k>
43. Tella, A.C.; Owalude, S.O.; Ojekanmi, C.A.; Oluwafemi, O.S.: Synthesis of copper-isonicotinate metal-organic frameworks simply by mixing solid reactants and investigation of their adsorptive properties for the removal of the fluorescein dye. *New J. Chem.* **38**(9), 4494–4500 (2014). <https://doi.org/10.1039/c4nj00411f>
44. Rabiei, M.; Palevicius, A.; Monshi, A.; Nasiri, S.; Vilkauskas, A.; Janusas, G.: Comparing methods for calculating nano crystal size of natural hydroxyapatite using X-ray diffraction. *Nanomaterials* **10**(9), 1–21 (2020). <https://doi.org/10.3390/nano10091627>
45. Alahmadi, M.; Alsaedi, W.H.; Mohamed, W.S.; Hassan, H.M.A.; Ezzeldien, M.; Abu-Dief, A.M.: Development of Bi₂O₃/MoSe₂ mixed nanostructures for photocatalytic degradation of methylene blue dye. *J. Taibah Univ. Sci.* **17**(1), 2161333 (2023). <https://doi.org/10.1080/16583655.2022.2161333>



46. Laila, A.M.A.-D.; Abdel-Rahman, H.; Rafat, S.M.A.-F.; El-Khatib, M.: Some new nano-sized Fe(II), Cd(II) and Zn(II) Schiff base complexes as precursor for metal oxides: sonochemical synthesis, characterization, DNA interaction, in vitro antimicrobial and anticancer activities. *Bioorg. Chem.* **69**, 140–156 (2016). <https://doi.org/10.1016/j.bioorg.2016.10.009>
47. Abu-dief, A.M.; Mohamed, W.S.: α -Bi₂O₃ nanorods: synthesis, characterization and UV-photocatalytic activity. *Mater. Res. Express* **4**, 035039 (2017)
48. Duan, S.; Huang, Y.: Electrochemical sensor using NH₂-MIL-88(Fe)-rGO composite for trace Cd²⁺, Pb²⁺, and Cu²⁺ detection. *J. Electroanal. Chem.* **807**, 253–260 (2017). <https://doi.org/10.1016/j.jelechem.2017.11.051>
49. Shagholani, H.; Ghoreishi, S.M.; Mousazadeh, M.: Improvement of interaction between PVA and chitosan via magnetite nanoparticles for drug delivery application. *Int. J. Biol. Macromol.* **78**(November 2017), 130–136 (2015). <https://doi.org/10.1016/j.ijbiomac.2015.02.042>
50. Aryee, A.A., et al.: Selective removal of anionic dyes in single and binary system using Zirconium and iminodiacetic acid modified magnetic peanut husk. *Environ. Sci. Pollut. Res.* (2021). <https://doi.org/10.1007/s11356-021-13030-5>
51. Tang, Y., et al.: Upconversion particles coated with molecularly imprinted polymers as fluorescence probe for detection of clenbuterol. *Biosens. Bioelectron.* **71**, 44–50 (2015). <https://doi.org/10.1016/j.bios.2015.04.005>
52. Zango, Z.U., et al.: Adsorption of chrysene in aqueous solution onto MIL-88(Fe) and NH₂-MIL-88(Fe) metal-organic frameworks: kinetics, isotherms, thermodynamics and docking simulation studies. *J. Environ. Chem. Eng.* **8**(2), 103544 (2020). <https://doi.org/10.1016/j.jece.2019.103544>
53. Wang, S.; Zhu, Z.H.; Coomes, A.; Haghseresh, F.; Lu, G.Q.: The physical and surface chemical characteristics of activated carbons and the adsorption of methylene blue from wastewater. *J. Colloid Interface Sci.* **284**(2), 440–446 (2005). <https://doi.org/10.1016/j.jcis.2004.10.050>
54. Seo, P.W.; Khan, N.A.; Hasan, Z.; Jung, S.H.: Adsorptive removal of artificial sweeteners from water using metal-organic frameworks functionalized with urea or melamine. *ACS Appl. Mater. Interfaces* **8**(43), 29799–29807 (2016). <https://doi.org/10.1021/acsami.6b11115>
55. Zango, Z.U.; Sambudi, N.S.; Jumbri, K.; Abu Bakar, N.H.H.; Saad, B.: Removal of pyrene from aqueous solution using Fe-based metal-organic frameworks. *IOP Conf. Ser. Earth Environ. Sci.* **549**(1), 012061 (2020). <https://doi.org/10.1088/1755-1315/549/1/012061>
56. Zango, Z.U., et al.: Removal of anthracene in water by MIL-88(Fe), NH₂-MIL-88(Fe), and mixed-MIL-88(Fe) metal-organic frameworks. *RSC Adv.* **9**(71), 41490–41501 (2019). <https://doi.org/10.1039/c9ra08660a>
57. Abu-Dief, A.M.; Abdel-Rahman, L.H.; Sayed, M.A.E.; Zikry, M.M.; Khalifa, M.E.; El-Metwaly, N.M.: Optimization strategy for green synthesis of silver nanoparticles (AgNPs) as catalyst for the reduction of 2,4-dinitrophenol via supported mechanism. *Appl. Phys. A* **128**, 592 (2022)
58. Abu-Dief, A.M.; Zikry, M.M.: Adsorption of the heavy metal ions onto bio sorbents: a review. *Int. J. Nanomater. Chem.* **4**(3), 27–39 (2018). <https://doi.org/10.18576/ijnc/040301>
59. Ahmed, I.; Jung, S.H.: Applications of metal-organic frameworks in adsorption/separation processes via hydrogen bonding interactions. *Chem. Eng. J.* **310**, 197–215 (2017). <https://doi.org/10.1016/j.cej.2016.10.115>
60. Song, J.Y.; Jung, S.H.: Adsorption of pharmaceuticals and personal care products over metal-organic frameworks functionalized with hydroxyl groups: quantitative analyses of H-bonding in adsorption. *Chem. Eng. J.* **322**, 366–374 (2017). <https://doi.org/10.1016/j.cej.2017.04.036>
61. Duan, C.; Wang, J.; Liu, Q.; Zhou, Y.; Zhou, Y.: Efficient removal of salbutamol and atenolol by an electronegative silanized β -cyclodextrin adsorbent. *Sep. Purif. Technol.* **282**, 120013 (2022). <https://doi.org/10.1016/j.seppur.2021.120013>
62. Lv, J., et al.: Effective removal of clenbuterol and ractopamine from water with a stable Al(III)-based metal-organic framework. *Inorg. Chem.* **60**(3), 1814–1822 (2021). <https://doi.org/10.1021/acs.inorgchem.0c03296>

Springer Nature or its licensor (e.g. a society or other partner) holds exclusive rights to this article under a publishing agreement with the author(s) or other rightsholder(s); author self-archiving of the accepted manuscript version of this article is solely governed by the terms of such publishing agreement and applicable law.